SC-RR-68-208

AEROSPACE NUCLEAR SAFETY

SC-RR-68-208
July 1968

CID # 3116

THERMAL ANALYSIS OF A SNAP-27 GRAPHITE FUEL CASK

D. W. Larson, 9513

AEROSPACE RADIOISOTOPE POWER
INFORMATION CENTER

Accession No.	Date
05407-02	AUG 28 1968

Sandia Laboratory

DO NOT DESTROY
Return to
AEROSPACE RADIOISOTOPE POWER
INFORMATION CENTER
Sandia Laboratory

SANDIA LABORATORIES

OPERATED FOR THE UNITED STATES ATOMIC ENERGY COMMISSION BY SANDIA CORPORATION | ALBUQUERQUE, NEW MEXICO; LIVERMORE, CALIFORNIA

Issued by Sandia Corporation,
a prime contractor to the
United States Atomic Energy Commission

LEGAL NOTICE

This report was prepared as an account of Government sponsored work. Neither the United States, nor the Commission, nor any person acting on behalf of the Commission:

A. Makes any warranty or representation, expressed or implied, with respect to the accuracy, completeness, or usefulness of the information contained in this report, or that the use of any information, apparatus, method, or process disclosed in this report may not infringe privately owned rights; or

B. Assumes any liabilities with respect to the use of, or for damages resulting from the use of any information, apparatus, method, or process disclosed in this report.

As used in the above, "person acting on behalf of the Commission" includes any employee or contractor of the Commission, or employee of such contractor, to the extent that such employee or contractor of the Commission, or employee of such contractor prepares, disseminates, or provides access to, any information pursuant to his employment or contract with the Commission, or his employment with such contractor.

SC-RR-68-208

THERMAL ANALYSIS OF A SNAP-27 GRAPHITE FUEL CASK

D. W. Larson, 9513
Sandia Laboratories, Albuquerque

Approved by: V. E. Blake, 9510

L. A. Hopkins, Jr., 9500

ABSTRACT

This report summarizes the thermal analysis conducted on a SNAP-27 graphite fuel cask and enclosed fuel capsule. The analysis was conducted to determine the feasibility of using a graphite cask to contain and protect the SNAP-27 fuel capsule during orbital decay and supercircular velocity lunar return trajectories for Apollo mission aborts.

July 1968

rj

SUMMARY

In the Aerospace Nuclear Safety Program, Sandia Laboratory is responsible for providing independent safety assessments of space nuclear power systems. These safety assessments require that the behavior of the nuclear systems be determined during all phases of its mission, including any mission aborts which might occur.

As part of the Aerospace Nuclear Safety Program, a number of aerodynamic and thermodynamic analyses of the SNAP-27 fuel cask and fuel capsule were conducted. This report summarizes the thermodynamic analysis that was performed on the SNAP-27 graphite fuel cask and enclosed fuel capsule. This study was part of the overall analysis used to determine the capability of the graphite fuel cask to protect the fuel capsule during mission aborts resulting in atmospheric reentry.

Three classes of mission aborts were analyzed, one at orbital decay velocity and two at supercircular velocities; the supercircular velocity reentries were at reentry angles of -6.4° and -38°. The results are shown as plots of temperature versus time for the graphite outer surface, fuel capsule outer liner, and fuel capsule inner liner for each of the atmospheric reentry trajectories considered. The effect of the graphite reaction kinetics upon the temperature response of the fuel capsule is shown to be small for all cases considered, but the effect of reaction kinetics on the temperature response of the graphite fuel cask is shown to be significant for the steep reentry angle supercircular velocity reentries.

TABLE OF CONTENTS

	Page
Introduction	9
Thermal Model	11
Aerodynamic Heating	15
Results	21
Conclusions	58
REFERENCES	62
APPENDIX A - Material Properties	63

LIST OF ILLUSTRATIONS

Figure		
1.	SNAP-27 Fuel Capsule	10
2.	SNAP-27 Graphite LM Fuel Cask (GLFC)	12
3.	Thermal Model	14
4.	Free Molecular-Continuum Heating Intersection	18
5.	Transition Drag Curve Comparison	23
6.	Temperature Response of GLFC and Fuel Capsule for Orbital Decay (Latitude 0°, Heading 32°, Sandia Drag Curve, Cp = 1.83)	31
7.	Temperature Response of GLFC and Fuel Capsule for Orbital Decay (Latitude 0°, Heading 32°, Sandia Drag Curve, Cp = 1.93)	32
8.	Temperature Response of GLFC and Fuel Capsule for Orbital Decay (Latitude 0°, Heading 32°, General Electric Drag Curve, Cp = 1.93)	33
9.	Temperature response of GLFC and Fuel Capsule for Orbital Decay (Latitude 32°, Heading 0°, Sandia Drag Curve, Cp = 1.83)	34
10.	Temperature Response of GLFC and Fuel Capsule for Orbital Decay (Latitude 32°, Heading 0°, Sandia Drag Curve, Cp = 1.93)	35

LIST OF ILLUSTRATIONS (cont)

Figure		Page
11.	Temperature Response of GLFC and Fuel Capsule for Orbital Decay (Latitude 32°, Heading 0°, General Electric Drag Curve, Cp = 1.93)	36
12.	Temperature Response of GLFC and Fuel Capsule from CMA-HERMAN Combination for Orbital Decay (Latitude 32°, Heading 0°, Sandia Drag Curve, Cp = 1.93)	37
13.	Temperature Response of Cask Surface for Orbital Decay By Three Separate Methods (Latitude 32°, Heading 0°, Sandia drag curve, Cp = 1.93)	38
14.	Temperature Difference Across Graphite During Orbital Decay	40
15.	Temperature Response of GLFC and Fuel Capsule for -6.4° Superorbital Velocity Reentry (Sandia Drag Curve, Cp = 1.83)	44
16.	Temperature Response of GLFC and Fuel Capsule for -6.4° Superorbital Velocity Reentry (Sandia Drag Curve, Cp = 1.93)	45
17.	Temperature Response of GLFC and Fuel Capsule for -6.4° Superorbital Velocity Reentry (General Electric Drag Curve, Cp = 1.93)	46
18.	Temperature Response of GLFC and Fuel Capsule from CMA-HERMAN Combination for -6.4° Superorbital Velocity Reentry (Sandia Drag Curve, Cp = 1.93)	47
19.	Temperature Response of Cask Surface for -6.4° Superorbital Velocity Reentry by Three Separate Methods	49
20.	Temperature Difference Across Graphite for -6.4° Superorbital Velocity Reentry	50
21.	Temperature Response of GLFC and Fuel Capsule for -38° Superorbital Velocity Reentry (Sandia Drag Curve, Cp = 1.83)	54
22.	Temperature Response of GLFC and Fuel Capsule for -38° Superorbital Velocity Reentry (Sandia Drag Curve, Cp = 1.93)	55
23.	Temperature Response of GLFC and Fuel Capsule for -38° Superorbital Velocity Reentry (General Electric Drag Curve, Cp = 1.93)	56
24.	Temperature Response of GLFC and Fuel Capsule from CMA-HERMAN Combination for -38° Superorbital Velocity Reentry	57

LIST OF ILLUSTRATIONS (cont)

Figure | Page

25. Temperature Response of Cask Surface for -38° Superorbital Velocity Reentry by Three Separate Methods 59

26. Temperature Difference Across Graphite for -38° Superorbital Velocity Reentry 60

LIST OF TABLES

TABLE

I. Thermal Model Description by Nodes 13

II. Thermal Model Initial Temperatures 22

III. Heating Rates to GLFC as a Function of Time and Altitude (Orbital Decay, LM Descent Tanks 80% Full, Latitude 0°, Heading 32°, Sandia Drag Curve, Cp = 1.83) 25

IV. Heating Rates to GLFC as a Function of Time and Altitude (Orbital Decay, LM Descent Tanks 80% Full, Latitude 0°, Heading 32°, Sandia Drag Curve, Cp = 1.93) 26

V. Heating Rates to GLFC as a Function of Time and Altitude (Orbital Decay, LM Descent Tanks 80% Full, Latitude 0°, Heading 32°, General Electric Drag Curve, Cp = 1.93) 27

VI. Heating Rates to GLFC as a Function of Time and Altitude (Orbital Decay, LM Descent Tanks 80% Full, Latitude 32°, Heading 0°, Sandia Drag Curve, Cp = 1.83) 28

VII. Heating Rates to GLFC as a Function of Time and Altitude (Orbital Decay, LM Descent Tanks 80% Full, Latitude 32°, Heading 0°, Sandia Drag Curve, Cp = 1.93). 29

VIII. Heating Rates to GLFC as a Function of Time and Altitude (Orbital Decay, LM Descent Tanks 80% Full, Latitude 32°, Heading 0°, General Electric Drag Curve, Cp = 1.93) 30

IX. Heating Rates to GLFC as a Function of Time and Altitude (-6.4° Superorbital Velocity Reentry, Sandia Drag Curve, Cp = 1.83) 41

X. Heating Rates to GLFC as a Function of Time and Altitude (-6.4° Superorbital Velocity Reentry, Sandia Drag Curve, Cp = 1.93) 42

XI. Heating Rates to GLFC as a Function of Time and Altitude, (-6.4° Superorbital Velocity Reentry, General Electric Drag Curve, Cp = 1.93) 43

XII. Heating Rates to GLFC as a Function of Time and Altitude, (-38° Superorbital Velocity Reentry, Sandia Drag Curve, Cp = 1.83) 51

LIST OF TABLES (cont)

TABLES Page

XIII. Heating Rates to GLFC as a Function of Time and Altitude (-38° Superorbital Velocity Reentry, Sandia Drag Curve, Cp = 1.93) 52

XIV. Heating Rates to GLFC as a Function of Time and Altitude (-38° Superorbital Velocity Reentry, General Electric Drag Curve, Cp = 1.93) 53

THERMAL ANALYSIS OF A SNAP-27 GRAPHITE FUEL CASK

Introduction

The SNAP-27 is a 56-watt thermoelectric power supply which will provide the power for the Apollo Lunar Surface Experiment Package (ALSEP) on the manned Apollo lunar missions. During the flight to the lunar surface the SNAP-27 fuel capsule (Figure 1) will be protected by the graphite LM fuel cask (GLFC) from the reentry environments of possible mission aborts.

As part of the Aerospace Nuclear Safety Program, Sandia Laboratory conducted aerodynamic and thermodynamic analyses of the SNAP-27 fuel cask and fuel capsule.[1,2] In Reference 2 it was shown that the SNAP-27 fuel cask and fuel capsule, as originally designed, would not survive all supercircular velocity lunar return reentries even if separated from the Lunar Module (LM) at high altitudes. The information contained in Reference 2 was presented at Atomic Energy Commission Headquarters by the Aerospace Nuclear Safety Department of Sandia Laboratory on November 4, 1966.

Probability information obtained by the Sandia Laboratory Safety Analysis Division indicated that the probability of mission aborts resulting in supercircular velocity reentries is of the same order of magnitude as those aborts leading to orbital decay reentries. Thus it became highly desirable to design a fuel cask which would survive both orbital decay and lunar return atmospheric reentries. The Space Electric Power Office (SEPO) of the AEC asked General Electric (GE) and Sandia Laboratory to study the feasibility of using a graphite cask to protect the SNAP-27 fuel capsule during mission abort reentries. The results of these studies were presented at AEC Headquarters by GE and Sandia Laboratory on January 5, 1967.[3] Based on the results of these studies, AEC/SEPO directed GE to redesign the SNAP-27 fuel cask to survive orbital decay and supercircular velocity reentries. GE subsequently redesigned the fuel cask based on a graphite heat shield.

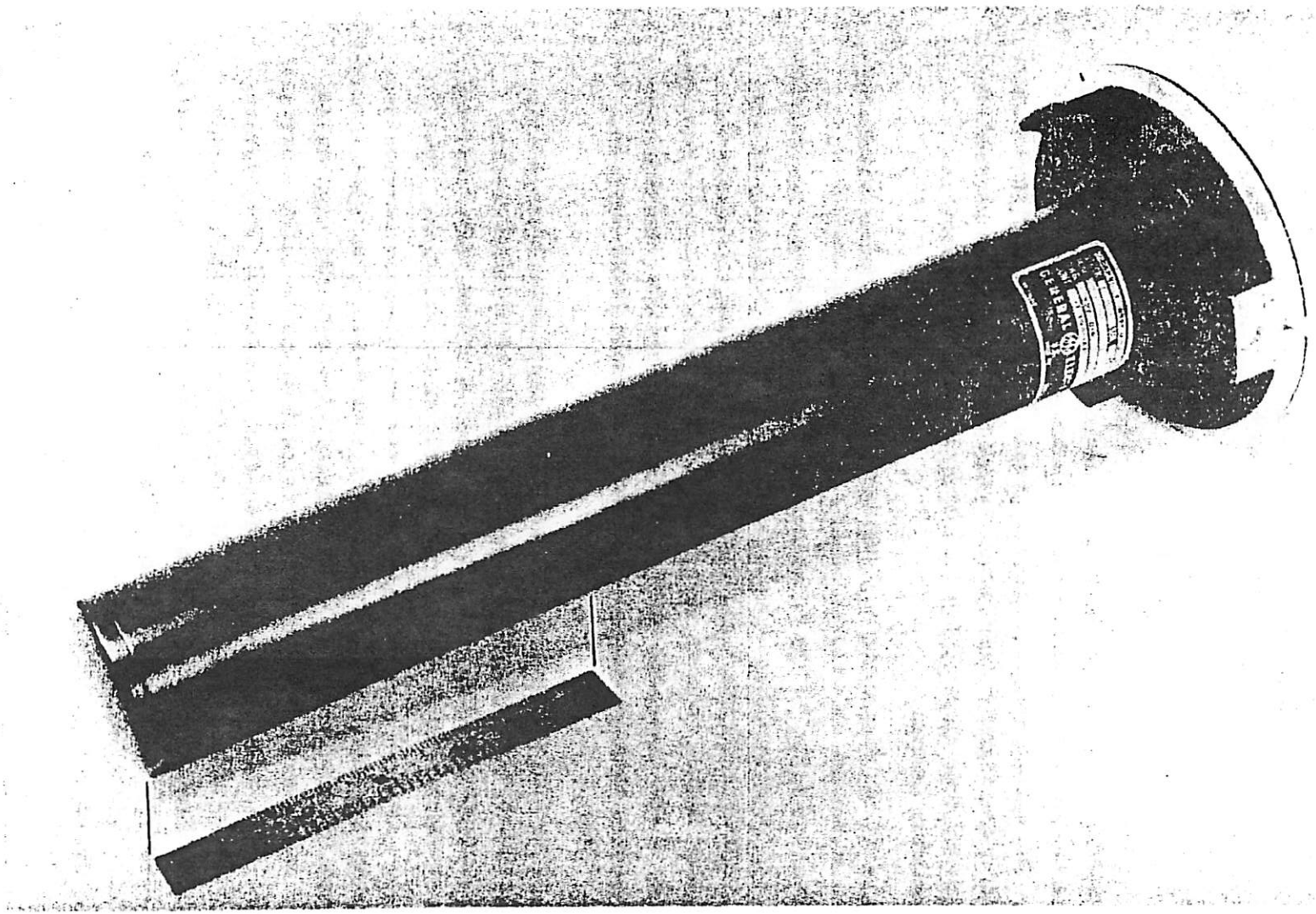

Figure 1. SNAP-27 Fuel Capsule

Preliminary aerodynamic and thermodynamic analyses conducted by Sandia Laboratory and GE indicated that the initial fuel cask redesign would not adequately protect the fuel capsule during some of the credible mission abort reentries. After a number of design revisions (A through F), preliminary analyses indicated adequate thermal protection of the fuel capsule had been attained. The final graphite cask design (Figure 2) is based on a graphite heat shield and a secondary thermal shield between the graphite shield and the fuel capsule.[4] During steady state conditions, the secondary thermal shield allows the internal heat generated by the fuel capsule to escape through the thermal shield by means of silver conduction fins which go through the secondary shield. In a reentry environment, the silver conduction fins melt and the secondary thermal shield then protects the fuel capsule from the high external heating rates to which the fuel cask is subjected.

An aerothermodynamic analysis of the SNAP-27 graphite fuel cask and fuel capsule was then conducted by Sandia Laboratory to determine the capability of the graphite fuel cask to protect the fuel capsule. Since this analysis is to be used to help determine the overall safety of the SNAP-27 fuel cask and fuel capsule on the manned Apollo lunar missions, this report has been written to document the thermal studies which were a part of the entire analysis.

Thermal Model

Introduction

The thermal model described in this section of the report was constructed for use in the Sandia HERMAN[5] heat transfer program and was run on Sandia's CDC 3600 computer. The material in which heat is flowing is broken up into a finite number of nodes. The mass of material associated with each node is treated as a lumped capacitance, and the material is partitioned such that the thermal parameters can be described by average values. When this is done, the thermal behavior of each node can be described by an ordinary differential equation. The system of differential equations is then solved simultaneously for each time step by a numerical integration technique. The program allows all thermal parameters to be varied as a function of time and/or temperature.

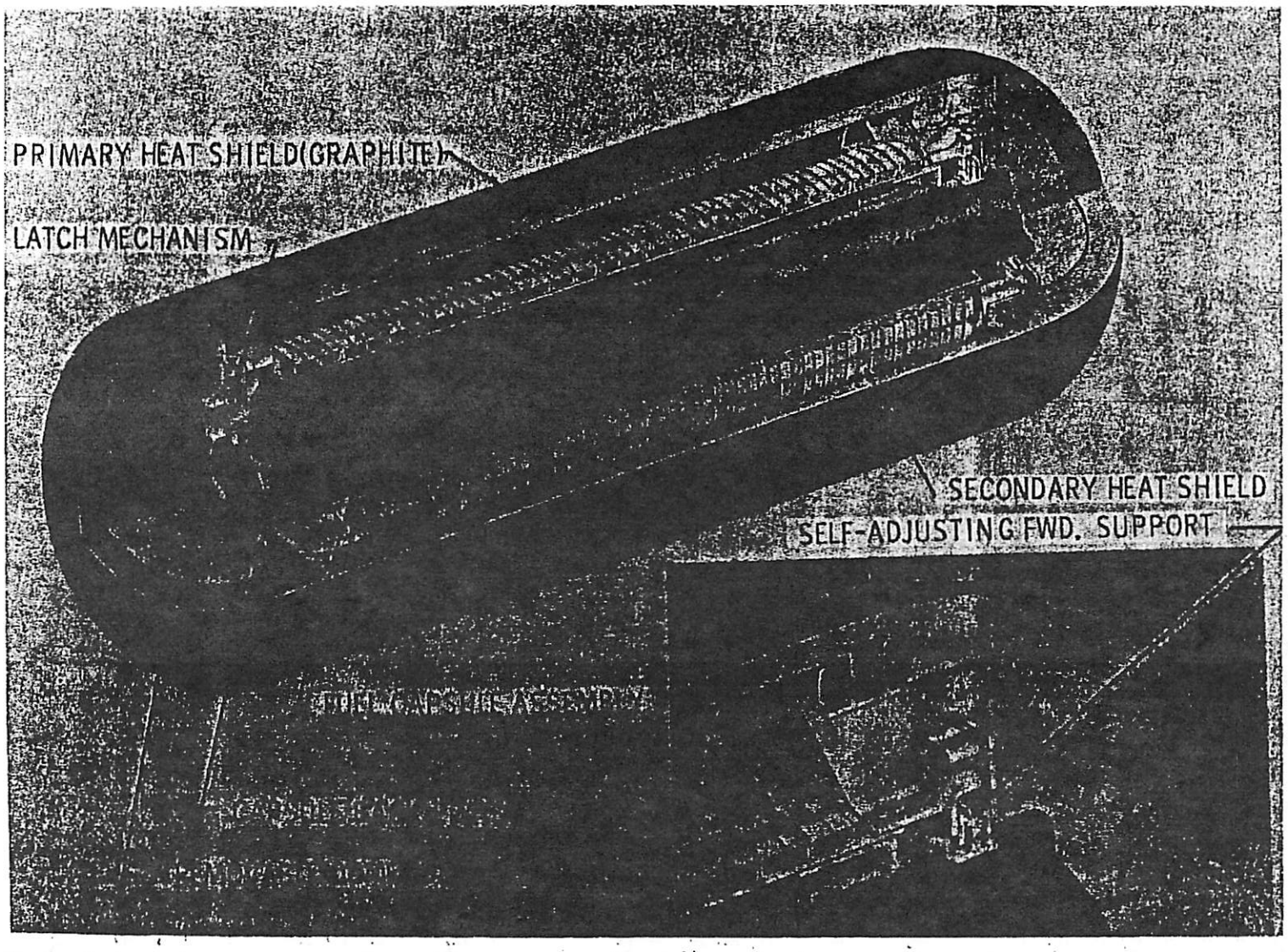

Figure 2. Graphite LM Fuel Cask (GLFC)

Model Description

The thermal model of the SNAP-27 graphite fuel cask and enclosed fuel capsule consists of a typical "slice" of the system one-half inch long. This representative portion of the system is divided into 16 nodes, as shown in Table I. The node numbers and relative node positions are shown in Figure 3. The material properties used in the model are given in Appendix A.

The thermal model is essentially one-dimensional with temperature gradients in the radial direction. However, in the secondary thermal shield, temperature gradients are allowed in both the radial and axial directions since the silver conduction fins create gradients in both directions. The model allows for heat transfer by conduction and for radiation between the appropriate nodes. All radiating surfaces are assumed to be gray with constant emissivities.

TABLE I

Thermal Model Description by Nodes

Component	Node No.	Node Material	Radial Distance (inches)	Node Thickness (inches)
Graphite Heat Shield	1	Graphite	4.00	0.05
	2	Graphite	3.89	0.12
	3	Graphite	3.77	0.13
	4	Graphite	3.67	0.05
Secondary Heat Shield	5	Silver	1.95	0.005
	6	Silver	1.95	0.005
	7	Silicon dioxide	1.90	0.10
	8	Silicon dioxide	1.90	0.10
	9	Silicon dioxide	1.80	0.10
	10	Silicon dioxide	1.80	0.10
	11	Silver and columbium	1.745	0.017
	12	Silver and columbium	1.745	0.017
Fuel Capsule	13*	Haynes 25	1.17	0.08
	14	Plutonium dioxide	0.98	0.20
	15	Plutonium dioxide	0.73	0.25
	16	Haynes 25	0.69	0.02

*Includes capsule cladding and fuel outer liner.

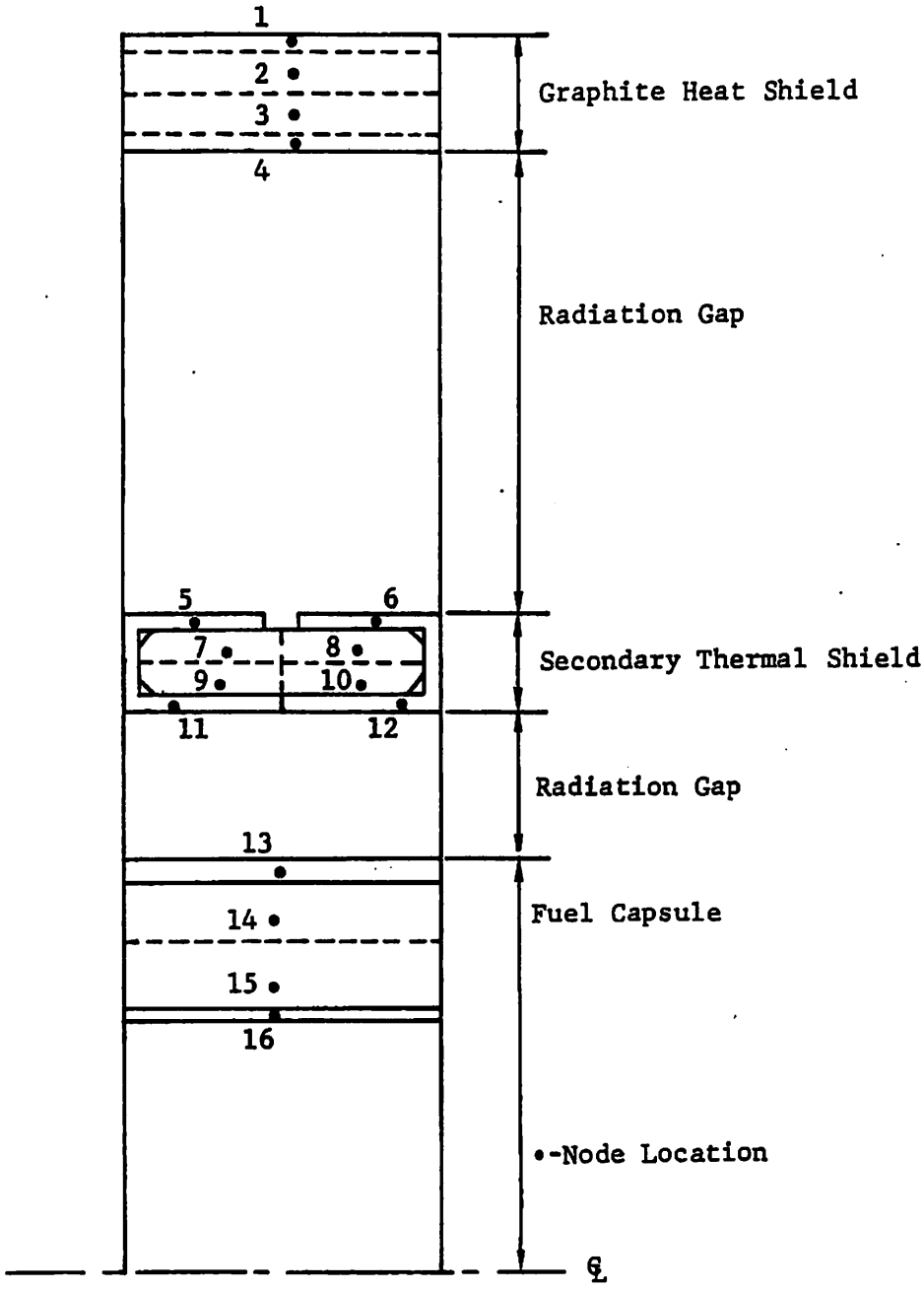

Figure 3. Thermal Model

The internal heat generated by the fuel capsule is included in the two fuel nodes. The aerodynamic heating is accounted for by applying a time-varying heat generation to the node nearest the graphite outer surface. The heat of fusion of the silver and the Haynes 25 is included in the model, and the conductance path provided by the silver fins goes to zero when the silver melts.

The radiant cooling during reentry is handled in the model by allowing the cask to radiate to a heat sink of constant temperature (400°R). The view factor of the graphite fuel cask (including end effects) to space while attached to the LM is 0.65. During reentry while the LM is still intact, the portion of the graphite cask exposed to aerodynamic heating has a view factor of 1.0. However, this value cannot be used for the entire cask prior to LM breakup or an unrealistic dip in temperature (below steady state) occurs. To circumvent this problem, the graphite cask is maintained at a steady state temperature until the aerodynamic heating to the cask is sufficient to counterbalance the sudden heat loss, and thus temperature drop, created when the view factor is switched from 0.65 to 1.0. At this time, the aerodynamic heat input is started and the view factor is changed to 1.0 simultaneously. Of course, this view factor is exactly correct after LM breakup.

Aerodynamic Heating

Introduction

During reentry into the atmosphere, the graphite fuel cask is subjected to high heating rates. The convective heat input occurs in both the free-molecular and continuum flow regimes. When the reentry velocity is sufficiently high, heat transfer to the cask also occurs by radiation from the high temperature gas cap formed in front of the reentering fuel cask. This section of the report indicates how the aerodynamic heat input to the cask is determined. In all cases, the rates are determined for the fuel cask spinning in cross flow as it reenters.

Convective Heating

The convective heat input to the cask in the free-molecular flow regime is determined by first calculating a reference heating rate to

a flat plate perpendicular to the flow. This reference heating rate is then related to the heating to the graphite fuel cask by a free-molecular heating ratio. The reference rate to the flat plate is readily determined by the equation

$$\dot{q} = \frac{a\ \rho_\infty\ V_\infty^3}{1556}\left(\frac{\text{BTU}}{\text{ft}^2\text{sec}}\right)$$

where

ρ_∞(slugs/ft^3)

V_∞(ft/sec) .

The accommodation coefficient, a, is defined by

$$a \equiv \frac{E_i - E_r}{E_i - E_w}$$

where

E_i = energy brought to the wall by incident molecules

E_r = energy carried away by reemitted molecules

E_w = energy that would be carried away if the reemitted molecules were at wall temperature.[6]

The accommodation coefficient for the graphite shield is taken to be 0.9. The free-molecular heating ratio for a cylinder in cross flow is determined in reference 6 to be a function of Mach number, and for the cases of interest to this report, it varies from 0.3197 to 0.3190.

In the continuum flow regime, the convective reference heating rate to a one-foot radius sphere is calculated by Sandia Corporation's Theoretical Trajectory Program A (TTA)[7] by the equation[12]

$$\dot{q}_c = 17600\left(\frac{\rho_\infty}{\rho_s}\right)^{1/2}\left(\frac{V_\infty}{V_c}\right)^{3.15}\ \text{BTU/ft}^2\text{-sec}$$

where

ρ_∞ is local air density

ρ_s is sea level air density

V_∞ is the air relative velocity

V_c is the circular orbital velocity.

This reference heating rate is then modified by a multiplier, Fq, to relate it to the actual heating rate to the graphite fuel cask. The multiplier is

$$Fq = \frac{1}{\sqrt{R}} (0.23) \quad ,$$

where R is the radius of the graphite fuel cask in feet. The factor 0.23 comes from two separate effects. The heating rate to the stagnation line on a cylinder is lower than that to a sphere of the same radius, due to the two-dimensional flow field around the cylinder and the three-dimensional flow field around the sphere. Flow theory indicates factors ranging from 0.707 to 0.74. Tests run at the Cornell Aeronautical Laboratory by R. D. Klett of Sandia Laboratory, indicated the heating rate reduction factor from a sphere to a cylinder to be 0.73. Since this was in good agreement with theory, the value 0.73 from the Cornell tests was used. The second effect occurs due to cylinder spin. The average heating around a cylinder was found to be 0.315 times the heat rate occuring along the cylinder stagnation line. Therefore, the average convective heat input to the SNAP-27 graphite fuel cask when it is reentering in a cross-flow spin mode is a factor of 0.398 of that continuum reference rate calculated by TTA.

The convective heat input calculated by TTA and corrected by the factors discussed above is the cold wall heat input and is further modified in the HERMAN program by the hot wall correction factor.

The convective heating which occurs in the transition flow regime is obtained by extending free molecular and continuum heating curves to their intersection, as shown for a specific orbital decay trajectory in Figure 4. This method is justified since it gives results close to the

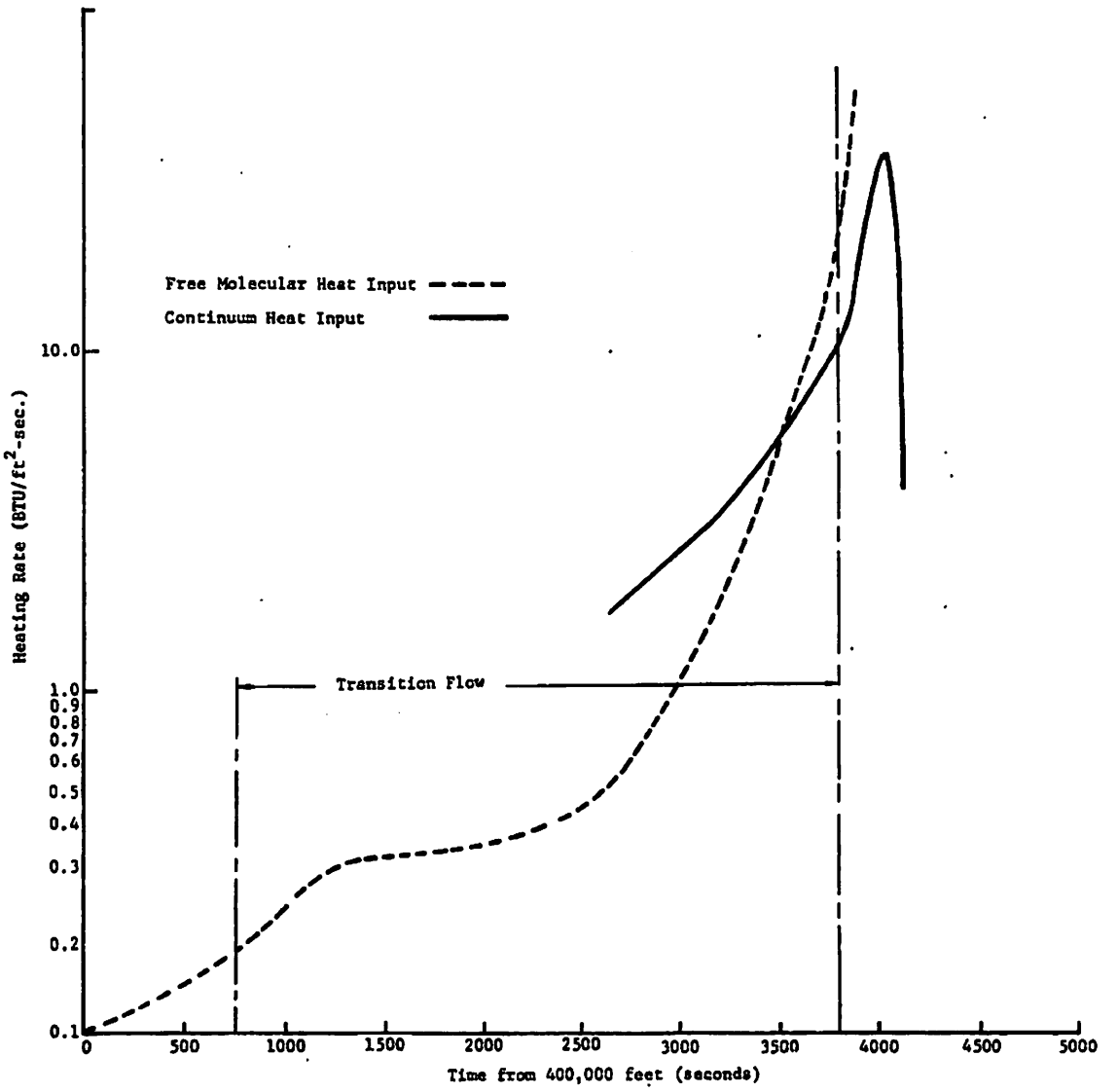

Figure 4. Free Molecular-Continuum Heating Intersection

various theories of transition flow heating as well as to experimental results.[6] As Figure 4 indicates, the intersection usually occurs toward the lower (continuum) end of transition flow.

Radiative Heating

When the reentry velocity is sufficiently high and remains so to altitudes where the air density is relatively high (<200,000 feet), a high temperature gas cap is formed in front of the reentering graphite fuel cask. The radiant heat transfer from the gas cap is then a significant portion of the total heat input to the cask. The TTA program calculates the radiant heat transfer ($\dot{q}_r$) to the stagnation point of a one foot radius sphere by use of the equation[12],

$$\dot{q}_r = A\left(\frac{\rho_\infty}{\rho_s}\right)^{1.78}\left(\frac{V_\infty}{10^4}\right)^B \quad \text{BTU/ft}^2\text{-sec}$$

where

ρ_∞ is local air density

ρ_s is sea-level air density

V_∞ is air relative velocity (ft/sec)

and where

$A = 6.8, \quad B = 12.5 \quad \text{for} \quad V_\infty < 30{,}000$

$A = .003, \quad B = 19.5 \quad \text{for} \quad 30{,}000 \le V_\infty \le 35000$

$A = 20.4, \quad B = 12.5 \quad \text{for} \quad 35{,}000 \le V_\infty$.

This value of radiant heat input is then modified by a radiant heating multiplier, F_r, to give the correct radiant heat input to the graphite cask when it is reentering in a cross-flow spin mode. F_r is determined by the equation,

$$F_r = 2\frac{R_c}{R_s}\,(0.188)$$

where

R_s is the radius of the sphere used in TTA (1 ft.)

R_c is the radius of the cylindrical section of the graphite fuel cask (0.33 ft.)

The factor 2 comes from the difference in the radiant heating to a stagnation point on a sphere to a stagnation line on a cylinder; this difference is caused by the difference in shock detachment distance. The factor 0.188 is the average radiant heating which occurs around the cylinder as compared to the radiant heating to the cylinder stagnation line.[8] Evaluation of F_r for the graphite fuel cask yields $F_r = 0.125$.

Reaction Kinetics

During atmospheric reentry, the actual heat input to the graphite heat shield is altered by the ablation and oxidation of the graphite surface. Since the HERMAN heat transfer program does not take these effects into account, one test case for each of the reentry conditions (orbital decay, -6.4° superorbital velocity reentry, and -38° superorbital velocity reentry) was run on Sandia's Charring Material Ablation Code (CMA).[11] This computer code determines the effect ablation and oxidation of the graphite have upon the heat input to the graphite wall, and it prints out the corrected heat input and the temperature difference across the graphite heat shield.

The corrected heat input to the graphite heat shield obtained from CMA is then used as input data to the HERMAN program. Comparisons can then be made from the HERMAN output as to how the temperatures are affected throughout the system with and without reaction kinetics taken into account. The temperature difference across the graphite heat shield is obtained directly from the CMA output without the necessity of going back through the HERMAN program. This difference is in fact more exact than that obtained from the HERMAN program since 10 material nodes are used across the graphite in CMA as compared to 4 in HERMAN. CMA also takes the receding surface effect (ablation) into account. The emissivity of the graphite was allowed to vary as a function of temperature in CMA, but it was held constant in HERMAN.

Results

Introduction

The SNAP-27 graphite fuel cask and fuel capsule temperature response during atmospheric reentry was determined for two orbital decay reentries and two supercircular velocity reentries. The initial temperature of each node of the thermal model is shown in Table II. Based on previous analyses of space systems reentering the atmosphere, the LM was expected to disassemble at 300,000 feet for the system decaying from orbit. For supercircular velocity reentries LM disassembly was expected at 330,000 feet, based upon flat plate free molecular heating and radiation equilibrium temperatures.[3] Therefore the ballistic coefficient for the LM was used down to those respective altitudes. Below those altitudes the graphite fuel cask and enclosed fuel capsule was assumed to be reentering in a cross-flow spin mode completely unencumbered.

The Sandia Reentry and Space Sciences Division and the GE Missile and Space Division have different transition drag curves for the graphite fuel cask (Figure 5). There was also some question concerning the correct value of the maximum pressure coefficient, Cp (1.83 as compared to 1.93).[9] Therefore, trajectories were computed for both orbital decay reentries and both supercircular velocity reentries with each of the pressure coefficients to determine their effect upon the temperature response of the fuel cask and fuel capsule.

Orbital Decay

The orbital decay reentry trajectories were computed for the following conditions:

A. Latitude 0°, Heading 32°, LM Descent Tanks 80 percent full.

   1. Sandia Drag Curve, Cp = 1.83
   2. Sandia Drag Curve, Cp = 1.93
   3. General Electric Drag Curve, Cp = 1.93

B. Latitude 32°, Heading 0°, LM Descent Tanks 80 percent full.

   1. Sandia Drag Curve, Cp = 1.83
   2. Sandia Drag Curve, Cp = 1.93
   3. General Electric Drag Curve, Cp = 1.93

TABLE II

Thermal Model Initial Temperatures

Node No.	Temperature (°R)
1	1245
2	1249
3	1253
4	1257
5	1566
6	1566
7	1564
8	1564
9	1574
10	1574
11	1582
12	1582
13	1834
14	2042
15	2204
16	2204

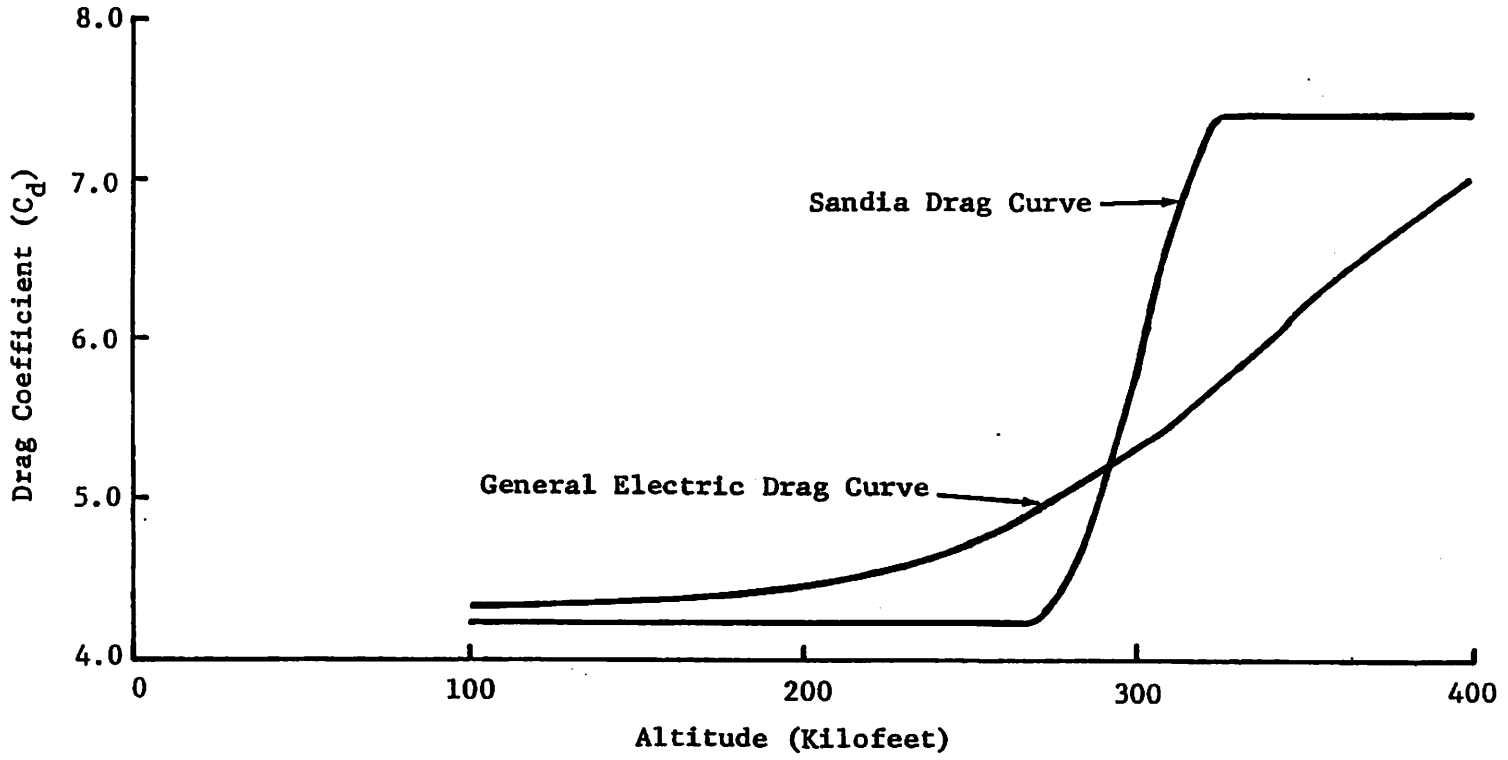

Figure 5. Transition Drag Curve Comparison

Some of the input data used for the thermal model for each of the above orbital decay cases are shown in Tables III through VIII, including time versus altitude, flow regime, convecting reference heating, heating rate multiplier (Fq), and cold wall heat input. Figures 6 through 11 show the temperature response of the fuel cask's outer surface and the fuel capsule's outer liner and inner liner for each of the above cases.

It can be seen from Figures 6 through 11 that the change in pressure coefficient has little effect on peak temperatures, with the higher pressure coefficient leading to peak graphite surface temperatures approximately 20°R cooler. It should be noted that the lower peak graphite surface temperatures generally leads to lower peak temperatures throughout the system; however, the peak temperature difference is not, in general, the same in a node to node comparison from one trajectory to another. The change in the drag curve has a slightly greater effect. The Sandia drag curve leads to peak temperatures on the graphite surface which are approximately 34°R higher than the GE drag curve. The different initial conditions at 400,000 feet altitude (Latitude 0°, Heading 32° compared to Latitude 32°, Heading 0°) leads to a large difference in trajectory time from 400,000 feet, but the peak temperatures reached throughout the system are essentially identical. Since the temperature differences are additive, the maximum temperature differences occur when the Sandia drag curve, low pressure coefficient trajectory is compared to the GE drag curve, high pressure coefficient trajectory. In the first case, the temperature is approximately 50°R higher on the graphite surface at peak temperature and approximately 40°R higher at the fuel capsule cladding. These temperature differences are relatively small at the temperatures involved (>2700°R).

The CMA computer code was used to determine the effect of ablation and oxidation for one orbital decay reentry trajectory (case B-2, page 21). The corrected heat flux obtained from CMA was used to input the HERMAN thermal model. Figure 12 shows the results. Figure 10 shows the results that were obtained from the HERMAN program alone. Comparison of the two figures indicates that the temperature response of the system is nearly identical for the two methods. The CMA-HERMAN combination leads to a peak temperature on the graphite surface 50°R higher than the HERMAN program alone. This is caused by the increased heat input from the graphite oxidation. Figure 13 compares three separate methods (HERMAN alone, CMA alone, CMA-HERMAN in combination) of predicting the graphite

TABLE III

Heating Rates to GLFC as a Function of Time and Altitude

Notes:
1. Orbital Decay, LM Descent Tanks 80% Full
2. Latitude 0° - Heading 32°
3. Sandia Drag Curve, Cp = 1.83

Flow Regime	Time (sec)	Altitude (ft)	Convective Reference Heating Rate (BTU/ft^2-sec)	Heating Rate Multiplier (Fq)	Accommodation Coefficient	Cold Wall Heat Input (BTU/ft^2-sec)
Free Molecular	0	400000	0.32	0.3197	0.9	0.09
	1140	406227	0.24	0.3197		0.07
	2010	390474	0.48	0.3196		0.14
	2490	379908	0.71	0.3195		0.20
	3480	380362	0.70	0.3195		0.20
	4110	370560	1.09	0.3195		0.31
	4380	360070	1.80	0.3194		0.52
	4590	350394	2.80	0.3194		0.80
	4800	340389	4.78	0.3193		1.37
	5010	330741	7.60	0.3193		2.18
	5250	320192	13.0	0.3193		3.74
	5460	310242	23.0	0.3193		6.61
Continuum	5630	299893	20.7	0.398	Not Applicable	8.24
	5740	289746	26.8			10.67
	5750	288446	28.0			11.14
	5890	255334	60.1			23.92
	5950	225172	89.2			35.50
	5970	210989	95.7			38.09
	5980	202870	96.7			37.61
	5990	193999	94.5			35.26
	6000	184357	88.6			24.95
	6020	162963	62.7			11.06
	6040	139992	27.8			5.73
	6050	128766	14.4			1.00
	6070	108376	2.5			0.06
	6100	82938	0.16			0
	6170	44231	0.01			0
	6370	80	0			

TABLE IV

Heating Rates to GLFC as a Function of Time and Altitude

Notes: 1. Orbital Decay, LM Descent Tanks 80% Full
2. Latitude 0° - Heading 32°
3. Sandia Drag Curve, Cp = 1.93

Flow Regime	Time (sec)	Altitude (feet)	Convective Reference Heating Rate (BTU/ft^2-sec)	Heating Rate Multiplier (Fq)	Accommodation Coefficient	Cold Wall Heat Input (BTU/ft^2-sec)
Free Molecular	0	400000	0.32	0.3197	0.9	0.09
	1140	406227	0.24	0.3197		0.07
	2010	390474	0.48	0.3196		0.14
	2490	379908	0.71	0.3195		0.20
	3480	380362	0.70	0.3195		0.20
	4110	370560	1.09	0.3195		0.31
	4380	360070	1.80	0.3194		0.52
	4590	350394	2.80	0.3194		0.80
	4800	340389	4.78	0.3193		1.37
	5010	330741	7.60	0.3193		2.18
	5250	320192	13.0	0.3193		3.74
	5460	310242	23.0	0.3193		6.61
Continuum	5630	299893	20.7	0.398	Not Applicable	8.24
	5740	289683	26.8			10.67
	5750	288363	28.0			11.14
	5890	254284	60.8			24.20
	5950	222816	89.2			35.50
	5970	207957	94.3			37.53
	5980	199455	93.1			37.05
	5990	190183	89.5			35.62
	6000	180149	81.1			32.27
	6020	158150	51.8			20.62
	6040	135189	19.4			7.72
	6050	124254	9.2			3.66
	6070	104638	1.42			0.57
	6100	80036	0.11			0.04
	6170	43441	0.01			0
	6370	546	0			0

TABLE V

Heating Rates to GLFC as a Function of Time and Altitude

Notes:
1. Orbital Decay, LM Descent Tanks 80% Full
2. Latitude 0° - Heading 32°
3. General Electric Drag Curve, Cp = 1.93

Flow Regime	Time (sec)	Altitude (feet)	Convective Reference Heating Rate (BTU/ft^2-sec)	Heating Rate Multiplier (Fq)	Accommodation Coefficient	Cold Wall Heat Input (BTU/ft^2-sec)
Free Molecular	0	400000	0.32	0.3197	0.9	0.09
	1140	406227	0.24	0.3197		0.07
	2010	390474	0.48	0.3196		0.14
	2490	379908	0.71	0.3195		0.20
	3480	380362	0.70	0.3195		0.20
	4110	370560	1.09	0.3195		0.31
	4380	360070	1.80	0.3194		0.52
	4590	350394	2.80	0.3194		0.80
	4800	340389	4.78	0.3193		1.37
	5010	330741	7.60	0.3193		2.18
	5250	320192	13.0	0.3193		3.74
	5460	310242	23.0	0.3193		6.61
Continuum	5630	299893	20.7	0.398	Not Applicable	8.24
	5740	289763	26.8			10.7
	5750	288465	27.9			11.1
	5890	254808	59.4			23.6
	5950	222868	85.1			33.9
	5960	215595	89.0			35.4
	5970	207610	90.1			35.9
	5980	198863	88.6			35.3
	5990	189326	84.5			33.6
	6000	179021	75.7			30.1
	6020	156568	46.5			18.5
	6040	133436	16.5			6.57
	6050	122558	7.56			3.01
	6070	103179	1.13			0.45
	6100	78920	0.10			0.04
	6170	43239	0.01			0
	6370	896	0			0

TABLE VI

Heating Rates to GLFC as a Function of Time and Altitude

Notes:
1. Orbital Decay, LM Descent Tanks 80% Full
2. Latitude 32° - Heading 0°
3. Sandia Drag Curve, Cp = 1.83

Flow Regime	Time (sec)	Altitude (feet)	Convective Reference Heating Rate (BTU/ft^2-sec)	Heating Rate Multiplier (Fq)	Accommodation Coefficient	Cold Wall Heat Input (BTU/ft^2-sec)
Free Molecular	0	400000	0.32	0.3197	0.9	0.09
	510	390071	0.49	0.3196		0.14
	870	379862	0.71	0.3195		0.20
	1410	369907	1.12	0.3195		0.32
	2640	360117	1.80	0.3194		0.52
	2880	350624	2.80	0.3194		0.80
	3090	339803	4.76	0.3193		1.37
	3240	330994	7.42	0.3193		2.13
	3420	319524	13.7	0.3193		3.94
	3570	309161	25.0	0.3193		7.18
Continuum	3690	299999	20.68	0.398	Not Applicable	8.23
	3790	290441	26.47			10.54
	3830	284974	30.77			12.25
	3890	273339	40.75			16.22
	3930	262149	52.55			20.91
	3960	251135	64.12			25.52
	4010	225279	88.88			35.37
	4030	211210	95.28			37.92
	4040	203146	96.34			38.34
	4050	194326	94.11			37.46
	4070	174399	77.82			30.97
	4090	151999	45.57			18.14
	4110	129222	14.81			5.89
	4130	108767	2.55			1.01
	4160	83268	0.17			0.07
	4250	37751	0			0
	4430	167	0			0

TABLE VII

Heating Rates to GLFC as a Function of Time and Altitude

Notes:
1. Orbital Decay, LM Descent Tanks 80% Full
2. Latitude 32° - Heading 0°
3. Sandia Drag Curve, Cp = 1.93

Flow Regime	Time (sec)	Altitude (feet)	Convective Reference Heating Rate (BTU/ft^2-sec)	Heating Rate Multiplier (Fq)	Accommodation Coefficient	Cold Wall Heat Input (BTU/ft^2-sec)
Free Molecular	0	400000	0.32	0.3197	0.9	0.09
	510	390071	0.49	0.3196		0.14
	870	379862	0.71	0.3195		0.20
	1410	369907	1.12	0.3195		0.32
	2640	360117	1.80	0.3194		0.52
	2880	350624	2.80	0.3194		0.80
	3090	339803	4.76	0.3193		1.37
	3240	330994	7.42	0.3193		2.13
	3420	319524	13.7	0.3193		3.94
	3570	309161	25.0	0.3193		7.18
Continuum	3690	299999	20.68	0.398	Not Applicable	8.23
	3790	290395	26.45			10.53
	3830	284842	30.80			12.26
	3890	272916	40.96			16.30
	3930	261357	52.99			21.09
	3960	249919	64.65			25.73
	4010	222895	88.86			35.37
	4020	215857	92.41			36.78
	4030	208138	93.86			37.36
	4040	199685	92.69			36.89
	4050	190459	89.22			35.51
	4070	169769	68.16			27.13
	4090	146994	35.02			13.94
	4110	124604	9.42			3.75
	4130	104940	1.47			0.59
	4160	80292	0.11			0.04
	4250	37219	0.007			0
	4430	619	0			0

TABLE VIII

Heating Rates to GLFC as a Function of Time and Altitude

Notes:
1. Orbital Decay, LM Tanks 80% Full
2. Latitude 32° - Heading 0°
3. General Electric Drag Curve, Cp = 1.93

Flow Regime	Time (sec)	Altitude (feet)	Convective Reference Heating Rate (BTU/ft^2-sec)	Heating Rate Multiplier (Fq)	Accommodation Coefficient	Cold Wall Heat Input (BTU/ft^2-sec)
Free Molecular	0	400000	0.32	0.3197	0.9	0.09
	510	390071	0.49	0.3196		0.14
	870	379862	0.71	0.3195		0.20
	1410	369907	1.12	0.3195		0.32
	2640	360117	1.80	0.3194		0.52
	2880	350624	2.80	0.3194		0.80
	3090	339803	4.76	0.3193		1.37
	3240	330994	8.42	0.3193		2.13
	3420	319524	13.7	0.3193		3.94
	3570	309161	25.0	0.3193		7.18
Continuum	3690	299999	20.7	0.398	Not Applicable	8.23
	3790	290453	26.5			10.55
	3830	284990	30.7			12.22
	3890	273270	40.5			16.12
	3930	261818	52.0			20.70
	3960	250342	63.1			25.11
	4010	222781	85.6			34.07
	4020	215539	88.7			35.3
	4030	207581	89.7			35.7
	4040	198859	88.2			35.10
	4050	189343	84.1			33.47
	4070	168089	62.4			24.84
	4090	144962	30.2			12.02
	4110	122619	7.6			3.02
	4130	103235	1.1			0.44
	4160	78972	0.1			0.04
	4250	37055	0.01			0
	4430	926	0			0

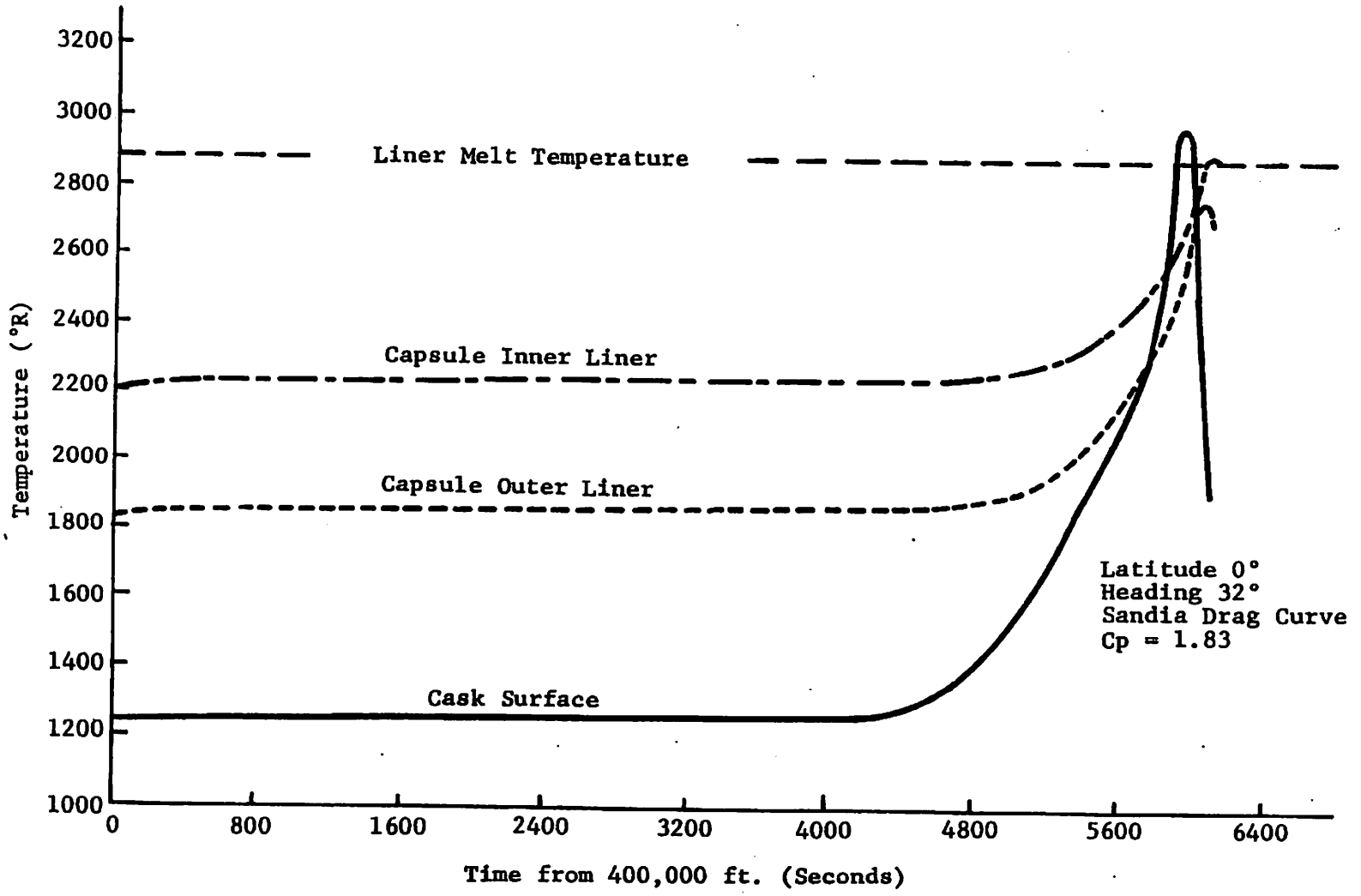

Figure 6. Temperature Response of GLFC and Fuel Capsule for Orbital Decay

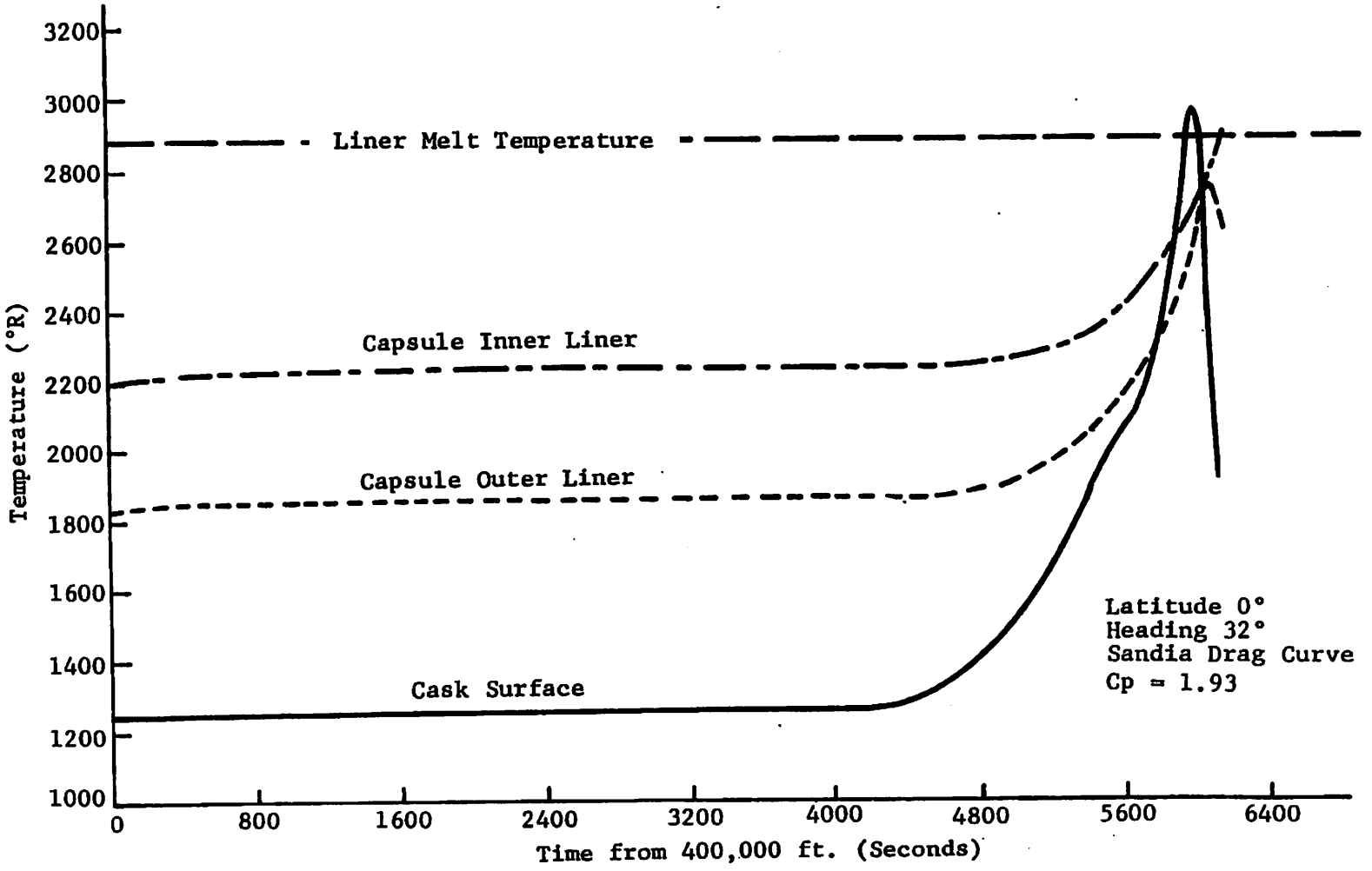

Figure 7. Temperature Response of GLFC and Fuel Capsule for Orbital Decay

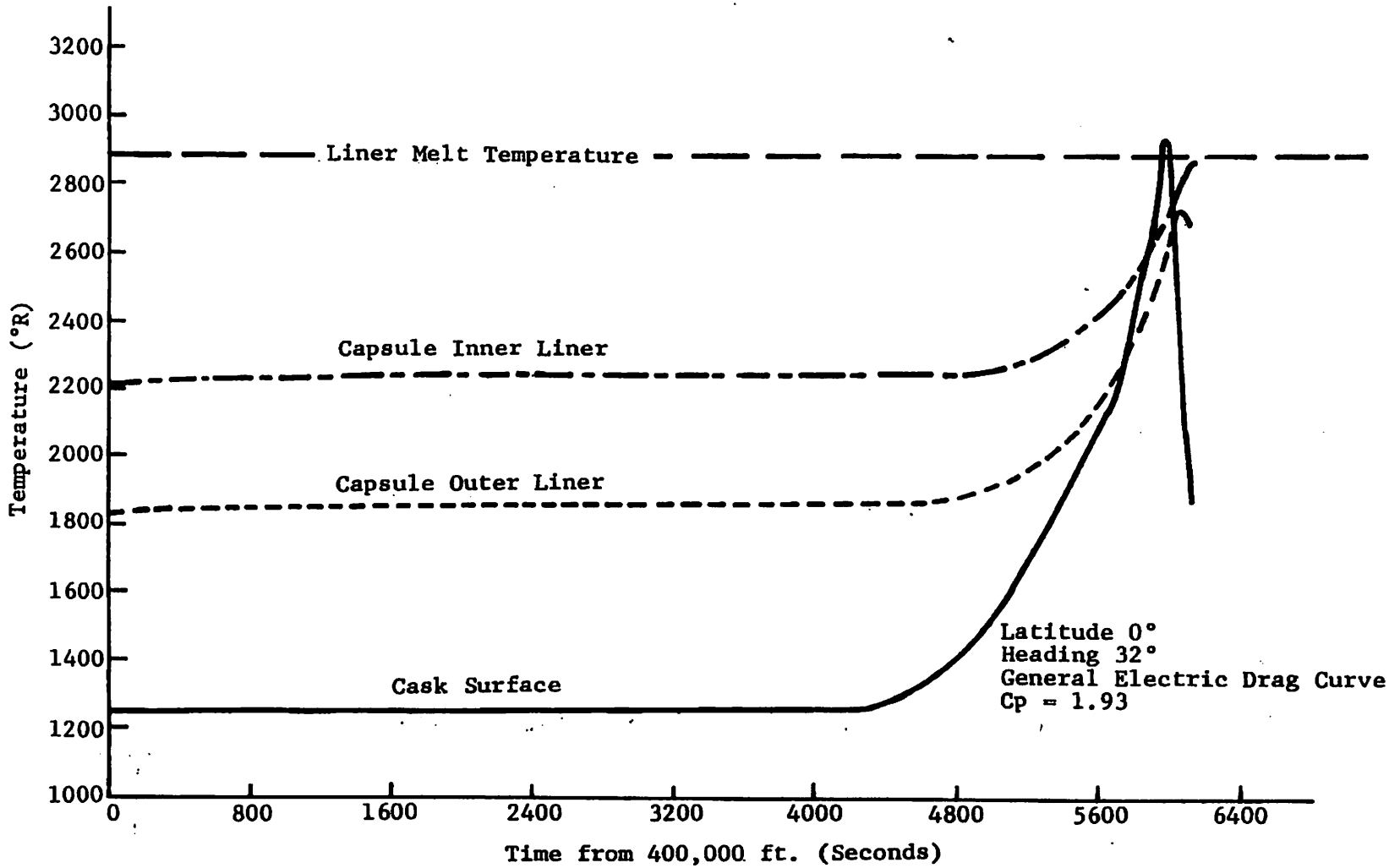

Figure 8. Temperature Response of GLFC and Fuel Capsule for Orbital Decay

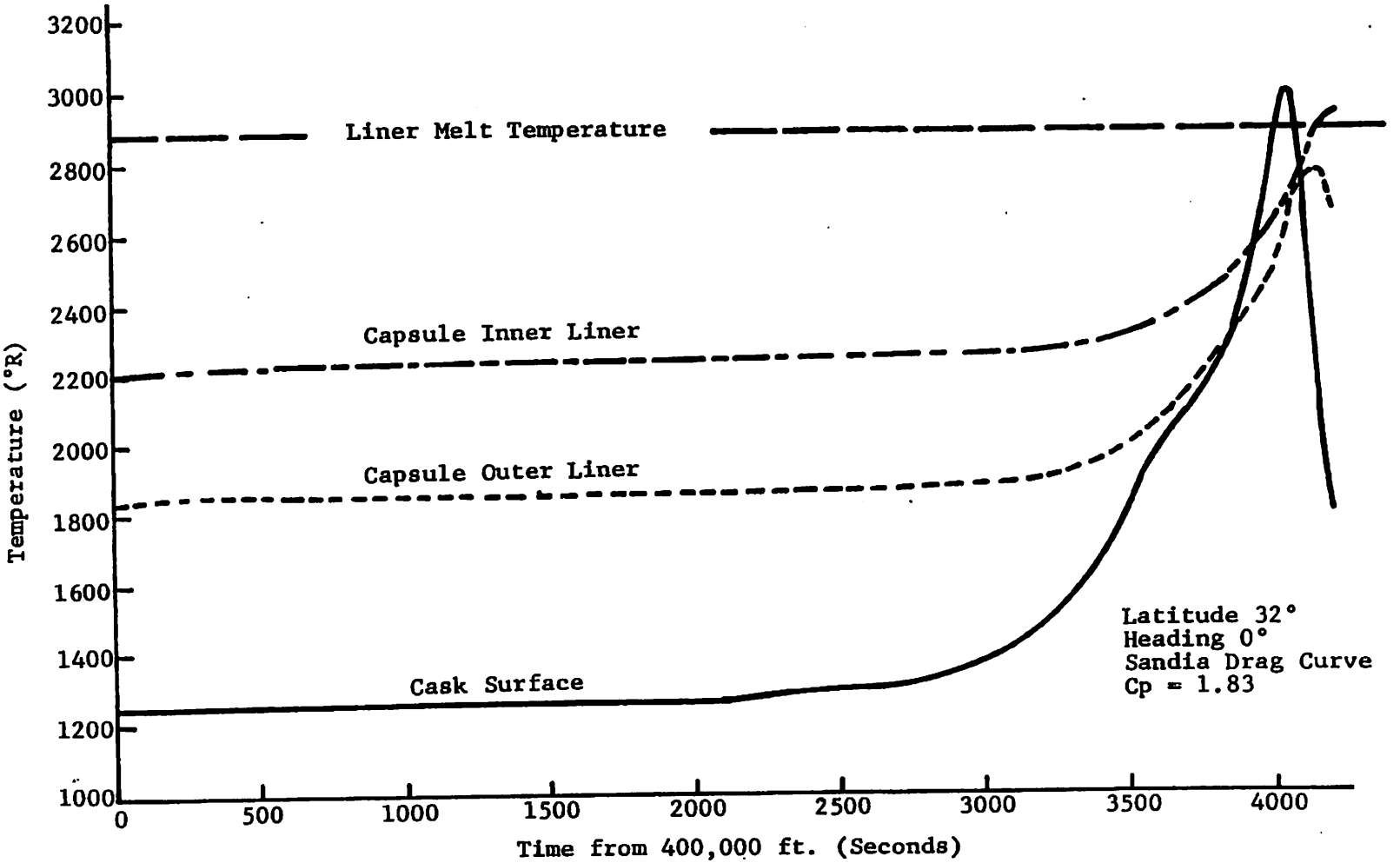

Figure 9. Temperature Response of GLFC and Fuel Capsule for Orbital Decay

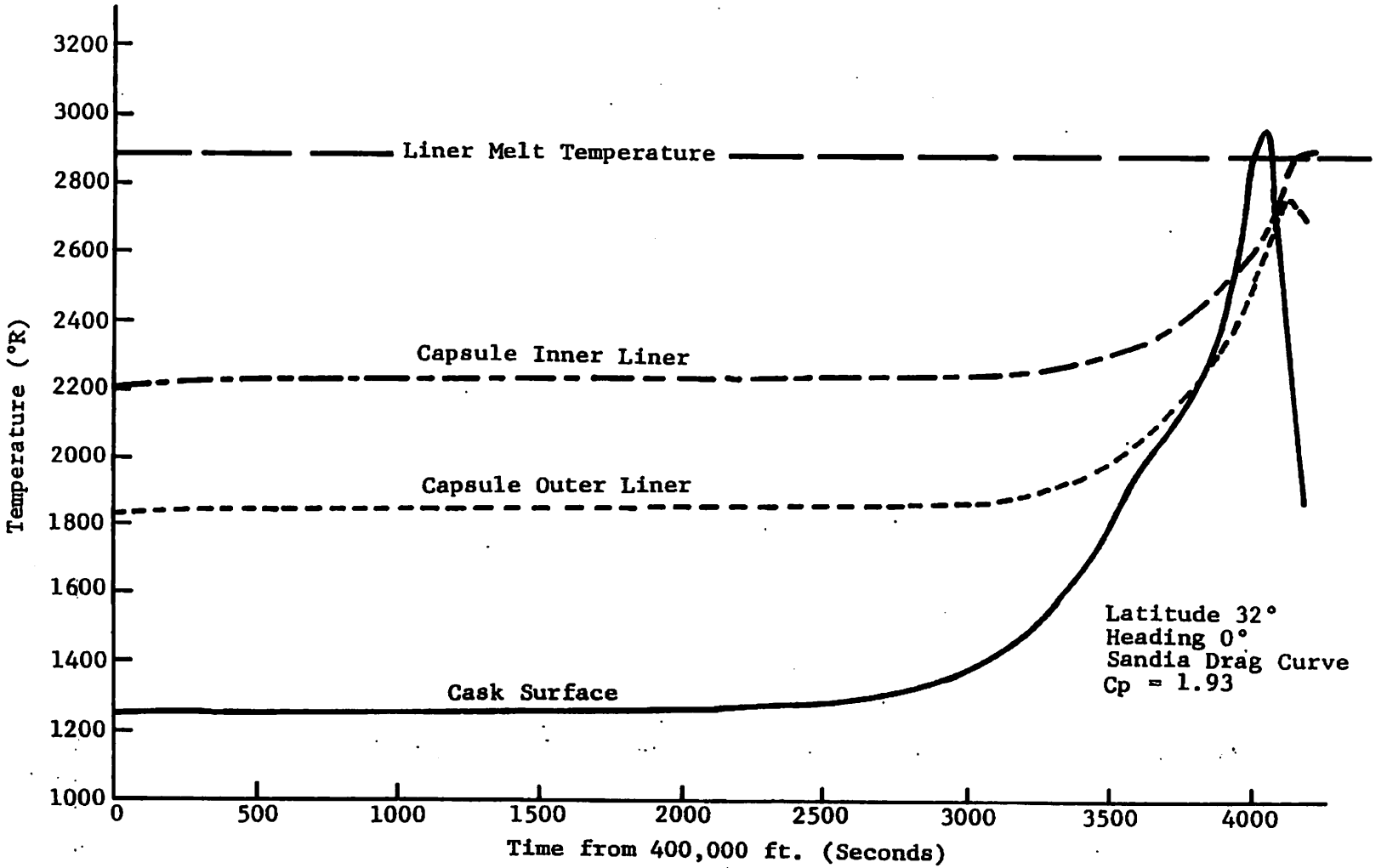

Figure 10. Temperature Response of GLFC and Fuel Capsule for Orbital Decay

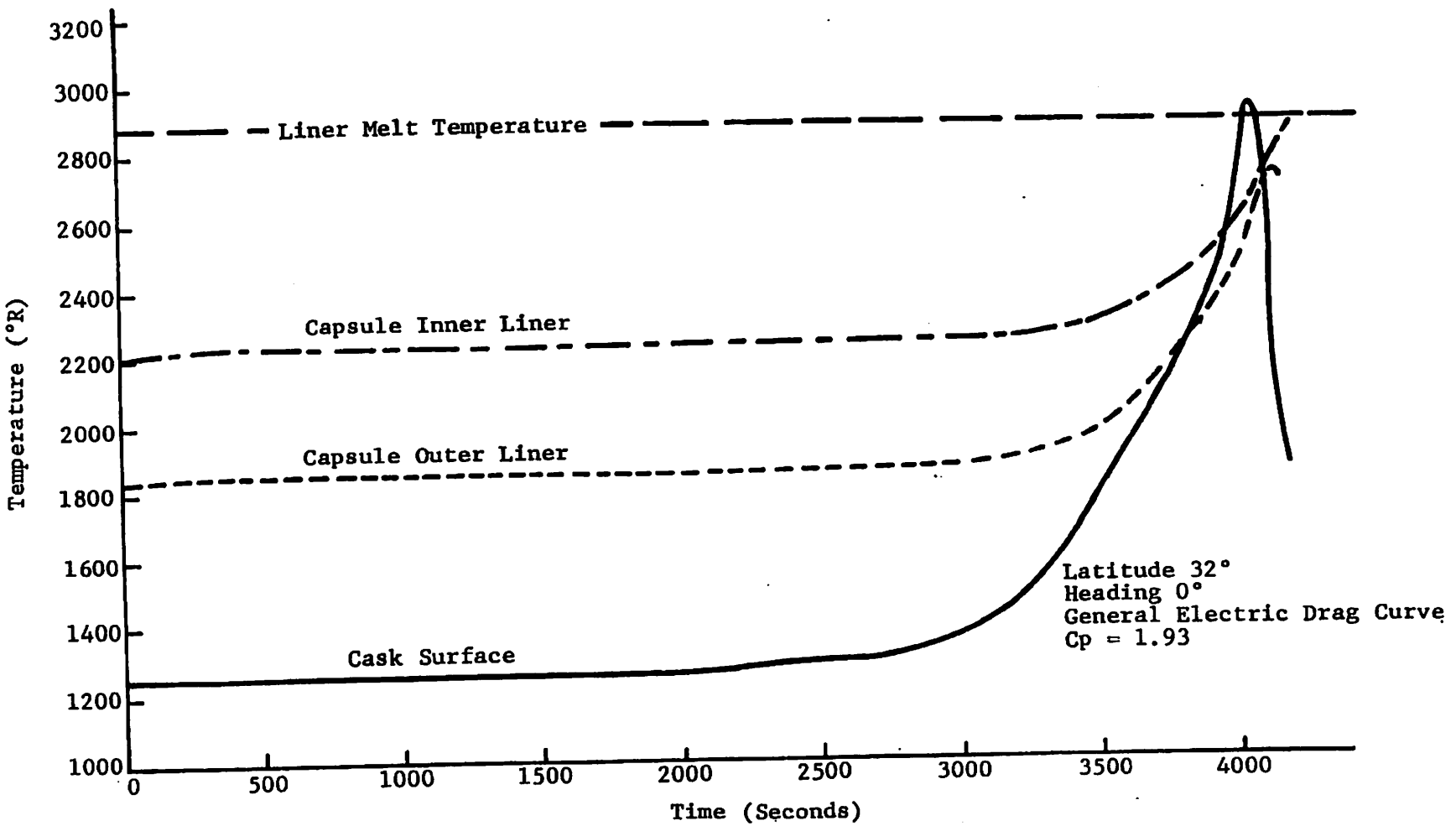

Figure 11. Temperature Response of GLFC and Fuel Capsule for Orbital Decay

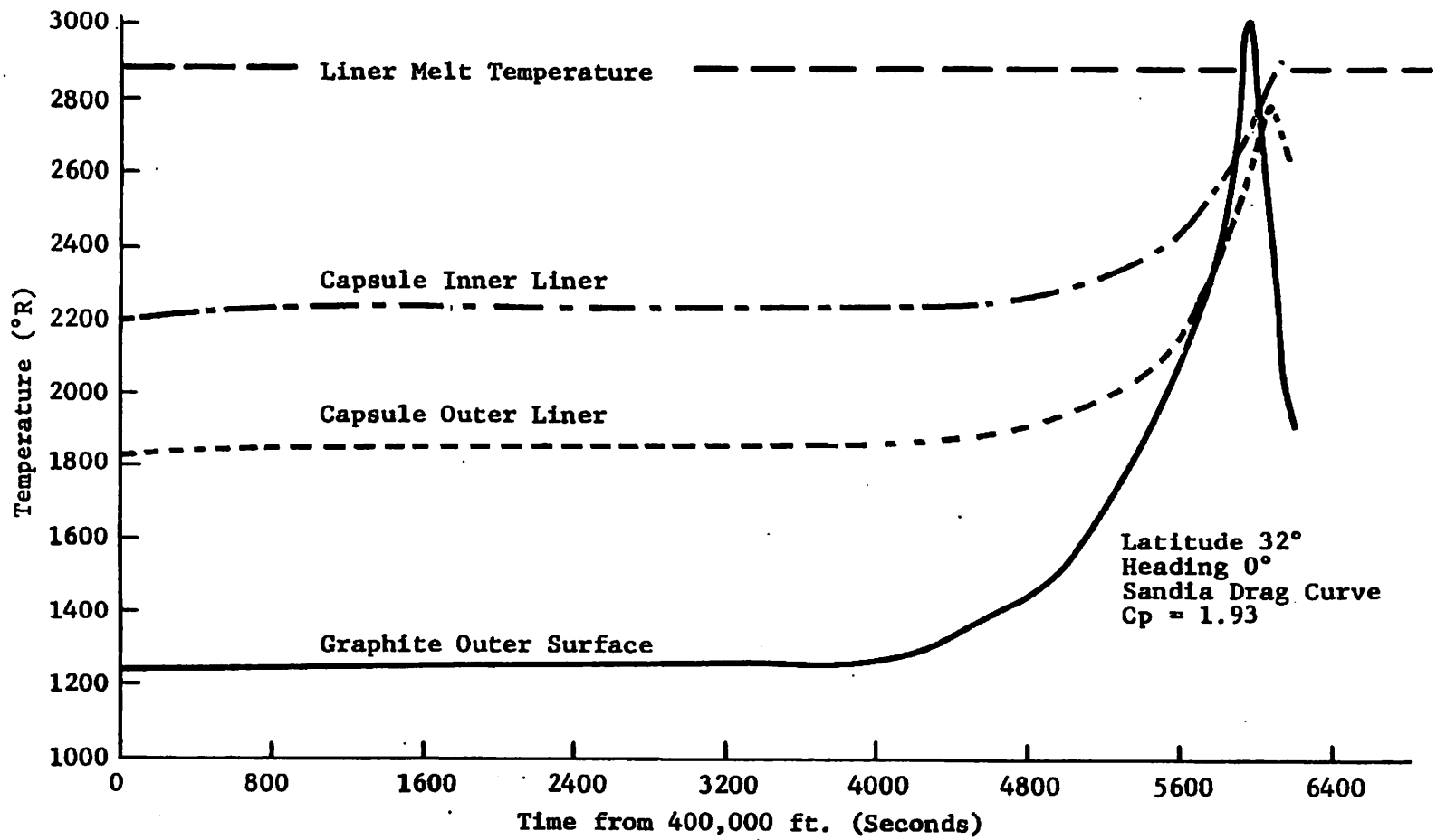

Figure 12. Temperature Response of GLFC and Fuel Capsule from CMA-HERMAN Combination

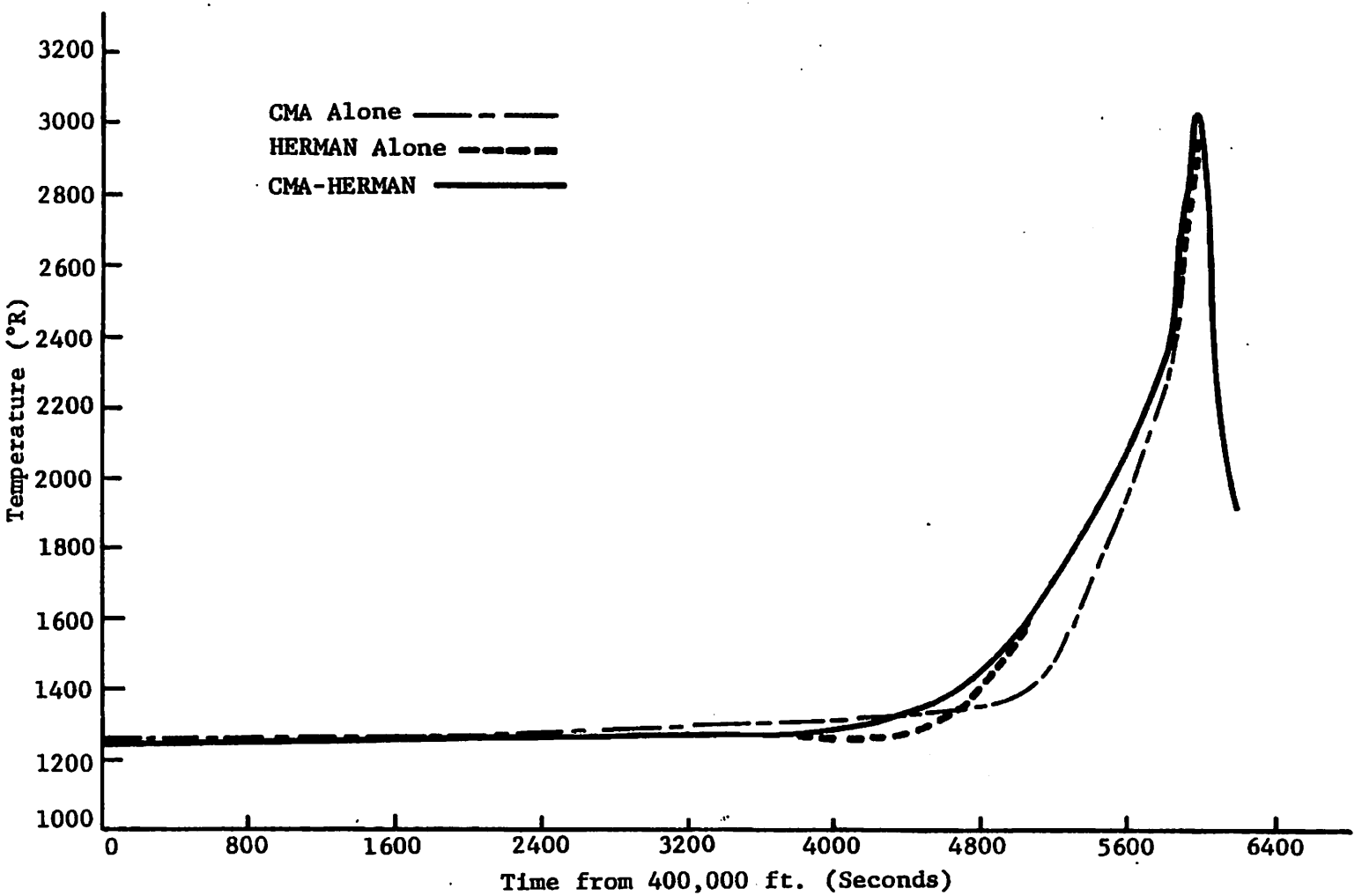

Figure 13. Temperature Response of Cask Surface for Orbital Decay by Three Separate Methods

cask surface temperature. Figure 14 shows the temperature difference across the graphite heat shield during orbital decay reentry as obtained directly from the CMA program. The temperature difference never exceeds 100°F for this trajectory.

-6.4 Degree Supercircular Velocity Reentry

A supercircular velocity reentry at a reentry angle of -6.4° was analyzed since this represents the desired reentry angle for a mission abort once the LM is inserted into a lunar trajectory.[10] These trajectories were computed for the following conditions:

-6.4° supercircular velocity reentry, LM ascent and descent tanks 100% full.

1. Sandia drag curve, Cp = 1.83
2. Sandia drag curve, Cp = 1.93
3. General Electric drag curve, Cp = 1.93

Some of the input data used for the thermal model for each of the above supercircular velocity reentry cases are shown in Tables IX, X, and XI. Included in the tables are time versus altitude, flow regime, convective reference heating, radiative reference heating, heating rate multiplier (Fq), and cold wall heat input. Figures 15, 16, and 17 show the temperature response of the graphite fuel cask outer surface, fuel capsule inner liner, and fuel capsule outer liner for each of the above cases.

These figures indicate that increasing the pressure coefficient from 1.83 to 1.93 causes the peak graphite temperature to decrease by approximately 30°R. This peak graphite temperature decreases another 40°R when the GE drag curve is used in place of the Sandia drag curve. The fuel capsule outer liner is also cooler by 31°R when the higher pressure coefficient and GE drag curve are used. These temperature differences are relatively small and indicate that either of the pressure coefficients or drag curves will give temperature responses which are very nearly the same.

The CMA computer code was used to determine the effect of ablation and oxidation on the temperature response of the system for a -6.4° supercircular velocity reentry trajectory. Figure 18 shows the temperature response of the system obtained by using the corrected heat flux from CMA as input to the HERMAN thermal model. Figure 16 shows

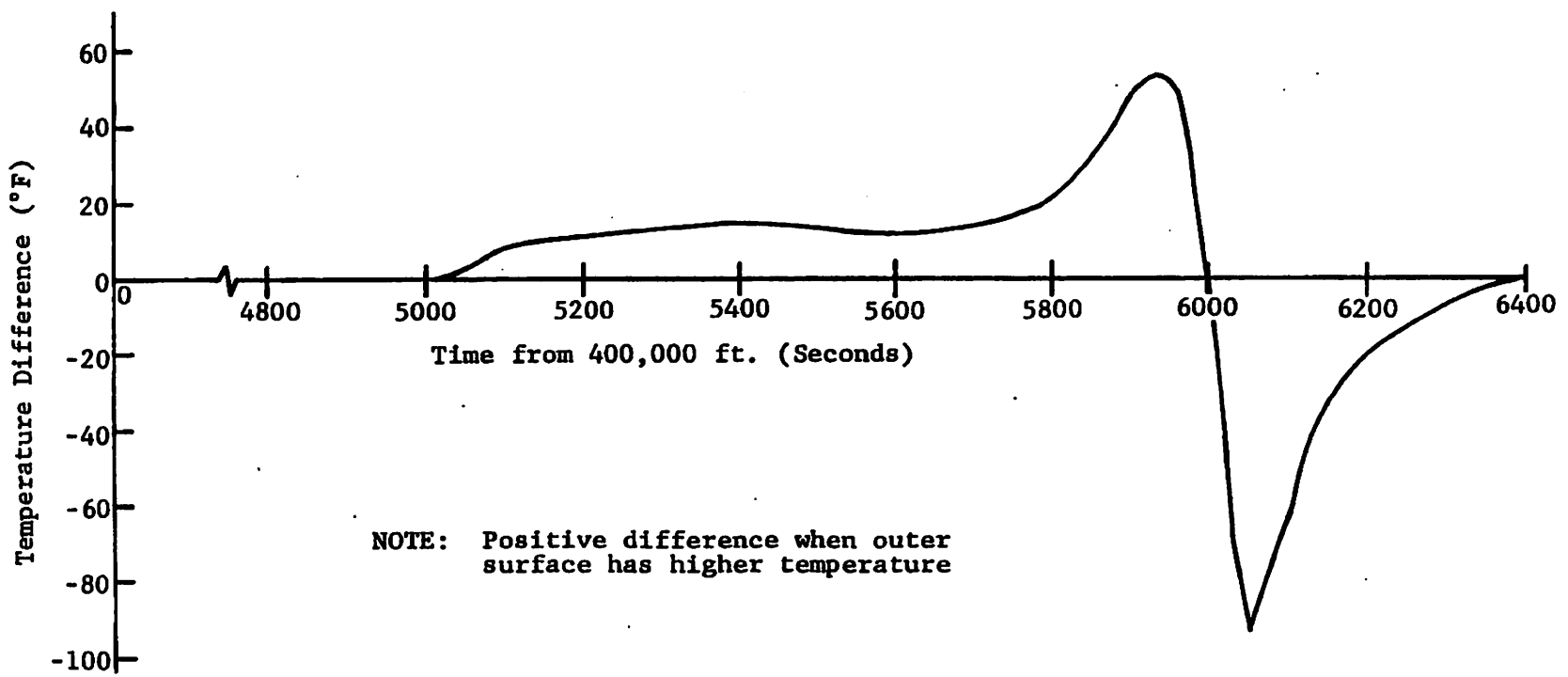

Figure 14. Temperature Difference Across Graphite During Orbital Decay

TABLE IX

Heating Rates to GLFC as a Function of Time and Altitude

-6.4° Superorbital Velocity Reentry
Sandia Drag Curve
Cp = 1.83

Flow Regime	Time (sec)	Altitude (feet)	Convective Reference Heating Rate (BTU/ft^2-sec)	Heating Rate Multiplier (Fq)	Accommodation Coefficient	Cold Wall Heat Input (BTU/ft^2-sec)
Free Molecular	0	400000	1.1	0.3192	0.9	0.316
	5	380602	2.4	0.3192		0.689
	10	361966	5.6	0.3192		1.61
	15	344096	12.6	0.3190		3.62
	20	326098	30.0	0.3190		8.61
	25	310653	76.0	0.3190		21.82
Continuum	30	295095	77.3	0.398	Not Applicable	30.77
	40	266340	171.2			68.14
	50	240828	299.6			119.2
	55	229341	365.7			145.5
	60	218733	423.6			168.6
	65	209014	462.8			184.2
	70	200176	477.3			190.0
	75	192184	470.4			187.2
	100	162007	200.6			79.84
	120	143533	56.5			22.49
	130	134688	26.5			10.55
	150	117130	4.9			1.95
	165	104218	1.3			0.52
	240	52708	0.02			0.008
	460	242	0			0

Radiant Heat Input

Time (sec)	Altitude (feet)	Reference Heating Rate (BTU/ft^2-sec)	Heating Rate Multiplier (F_r)	Radiant Heat Input (BTU/ft^2-sec)
50	240828	1.88	0.125	0.24
55	229341	3.44		0.43
60	218733	4.92		0.62
65	209014	5.28		0.66
70	200176	4.22		0.53
75	192184	2.91		0.36
80	184975	2.04		0.26

TABLE X

Heating Rates to GLFC as a Function of Time and Altitude

-6.4° Superorbital Velocity Reentry
Sandia Drag Curve
Cp = 1.93

Flow Regime	Time (sec)	Altitude (feet)	Convective Reference Heating Rate (BTU/ft^2-sec)	Heating Rate Multiplier (Fq)	Accommodation Coefficient	Cold Wall Heat Input (BTU/ft^2-sec)
Free Molecular	0	400000	1.1	0.3192	0.9	0.316
	5	380602	2.4	0.3192		0.689
	10	361966	5.6	0.3192		1.61
	15	344094	12.6	0.3190		3.62
	20	326988	30.0	0.3190		8.61
	25	310653	76.0	0.3190		21.82
Continuum	30	295096	77.3	0.398	Not	30.77
	40	266344	171.0		Applicable	68.06
	50	240840	298.7			118.9
	55	229364	363.8			144.8
	60	218770	419.9			167.1
	65	209070	456.5			185.3
	70	200255	468.1			186.3
	75	192287	457.9			182.2
	80	185102	420.8			167.5
	100	162179	186.9			74.4
	120	143669	51.16			20.36
	130	134805	23.74			9.45
	150	117240	4.35			1.73
	165	104350	1.12			0.45
	240	53269	0.02			0
	460	1343	0			0

Radiant Heat Input

Time (sec)	Altitude (feet)	Reference Heating Rate (BTU/ft^2-sec)	Heating Rate Multiplier (F_r)	Radiant Heat Input (BTU/ft^2-sec)
50	240840	1.85	0.125	0.231
55	229364	3.34		0.417
60	218770	4.66		0.538
65	209070	4.87		0.609
70	200255	3.75		0.469
75	192287	2.61		0.326
80	185102	1.77		0.221

TABLE XI

Heating Rates to GLFC as a Function of Time and Altitude

-6.4° Superorbital Velocity Reentry
General Electric Drag Curve
Cp = 1.93

Flow Regime	Time (sec)	Altitude (feet)	Convective Reference Heating Rate (BTU/ft^2-sec)	Heating Rate Multiplier (Fq)	Accommodation Coefficient	Cold Wall Heat Input (BTU/ft^2-sec)
Free Molecular	0	400000	1.1	0.3192	0.9	0.316
	5	380602	2.4	0.3192		0.689
	10	361966	5.6	0.3192		1.61
	15	344094	12.6	0.3190		3.62
	20	326988	30.0	0.3190		8.61
	25	310653	76.0	0.3190		21.82
Continuum	30	295094	77.3	0.398	Not	30.77
	40	266342	170.9		Applicable	68.02
	50	240859	296.8			118.1
	55	229407	359.5			143.1
	60	218844	412.4			164.1
	65	209181	445.3			177.3
	70	200400	453.8			180.6
	75	192460	440.9			175.9
	80	185292	402.8			160.3
	85	178806	349.1			138.9
	100	162321	175.6			69.89
	120	143657	47.7			18.98
	130	134723	22.1			8.80
	150	117088	4.0			1.59
	165	104199	1.02			0.41
	240	53465	0.02			0.008
	470	385	0			0

Radiant Heat Input

Time (sec)	Altitude (feet)	Reference Heating Rate (BTU/ft^2-sec)	Heating Rate Multiplier (Fr)	Radiant Heat Input (BTU/ft^2-sec)
30	295094	0	0.125	0
50	240859	1.78		0.22
55	229407	3.11		0.39
60	218844	4.19		0.52
65	209181	4.19		0.52
70	200400	3.11		0.39
75	192460	2.25		0.28
80	185292	1.49		0.19
100	1623321	0		0

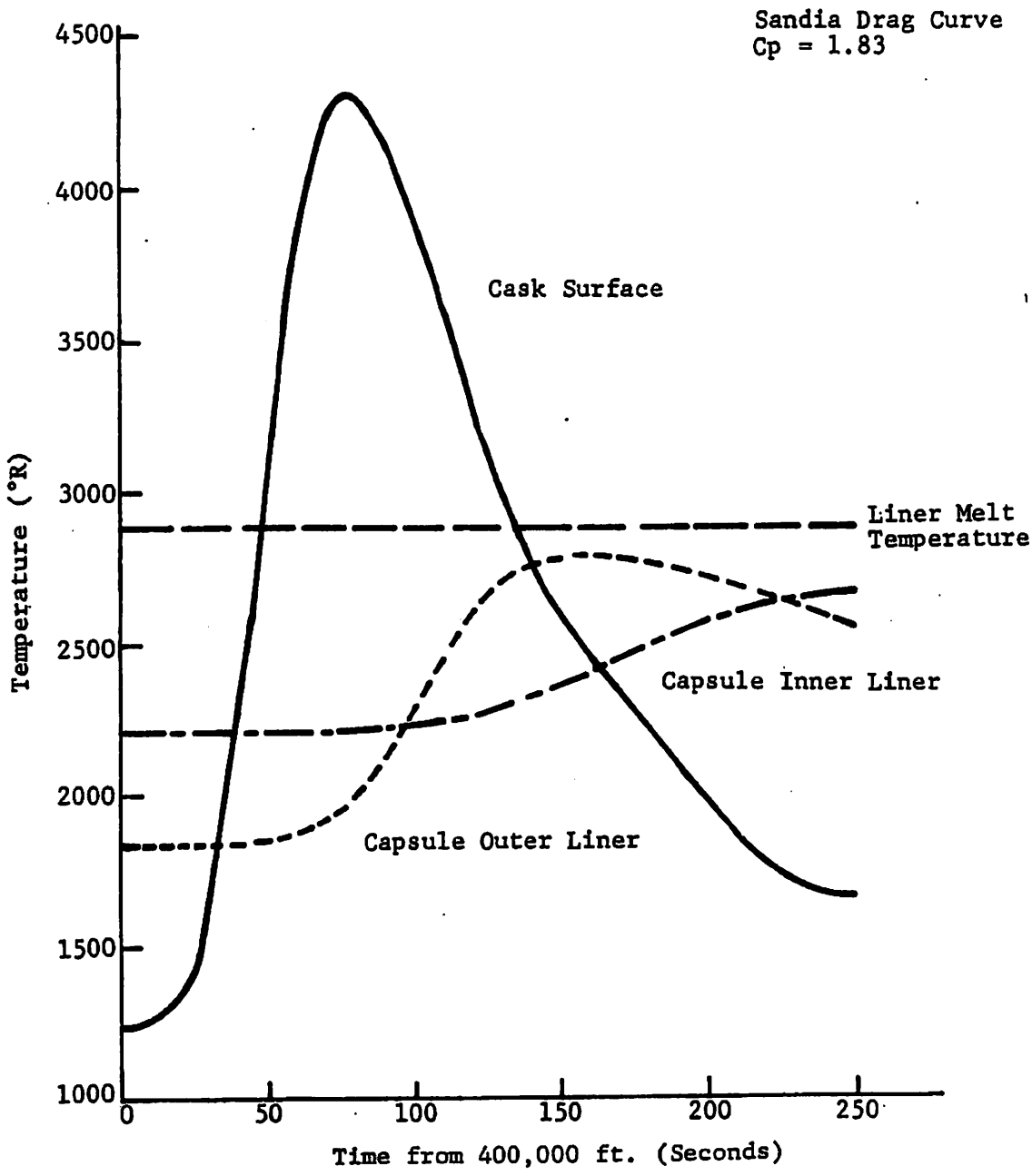

Figure 15. Temperature Response of GLFC and Fuel Capsule for -6.4° Superorbital Velocity Reentry

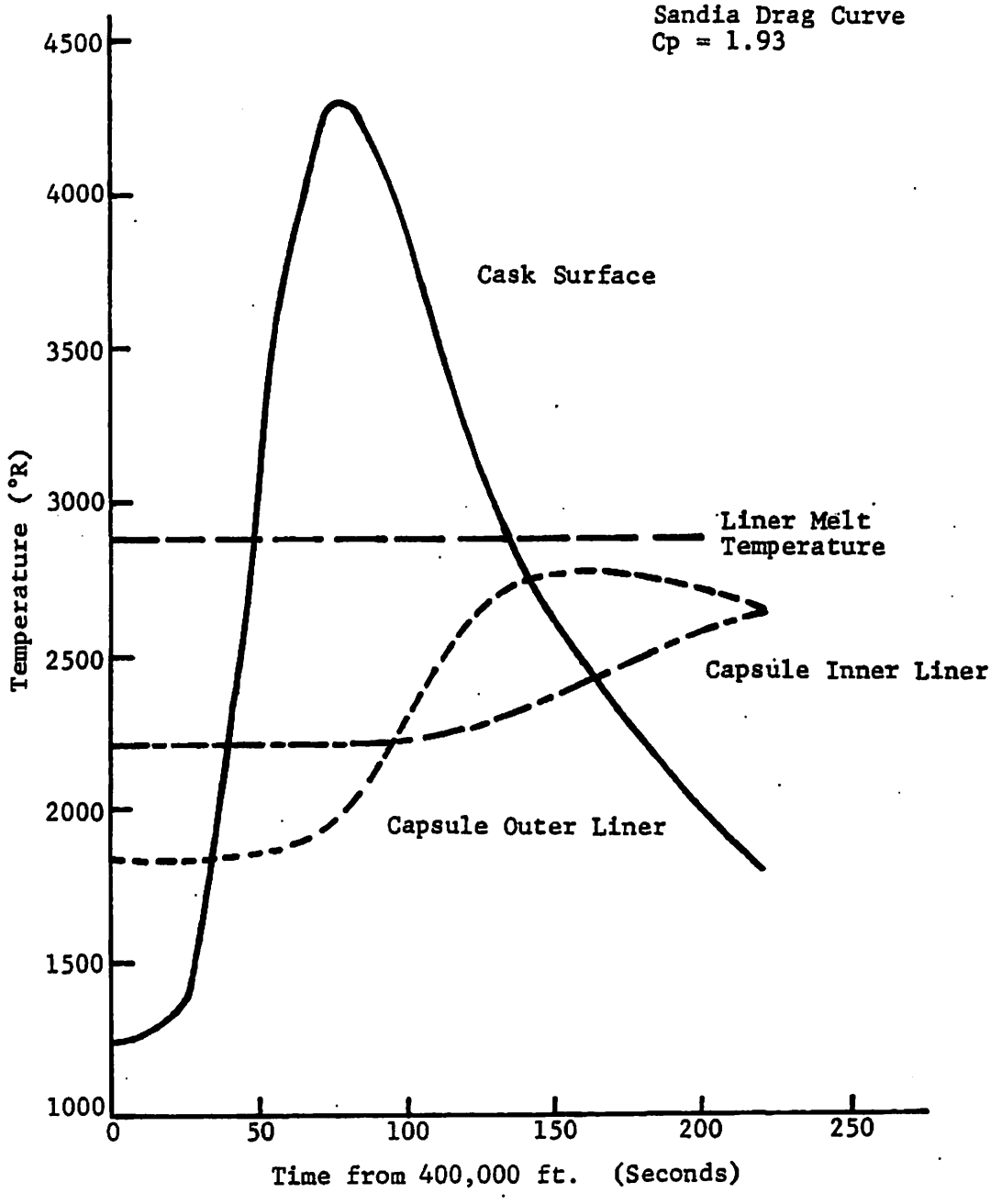

Figure 16. Temperature Response of GLFC and Fuel Capsule for -6.4° Superorbital Velocity Reentry

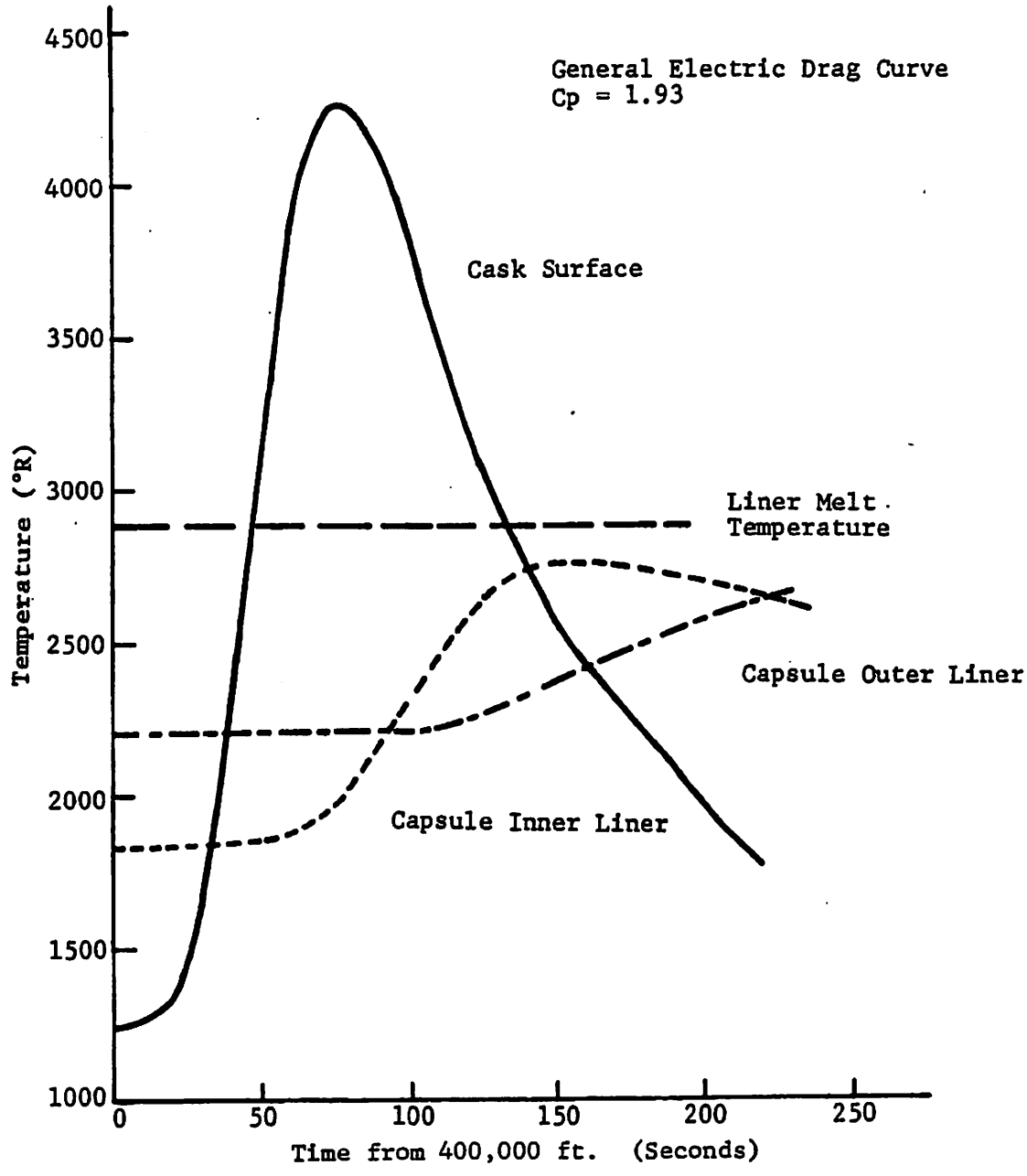

Figure 17. Temperature Response of GLFC and Fuel Capsule for -6.4° Superorbital Velocity Reentry

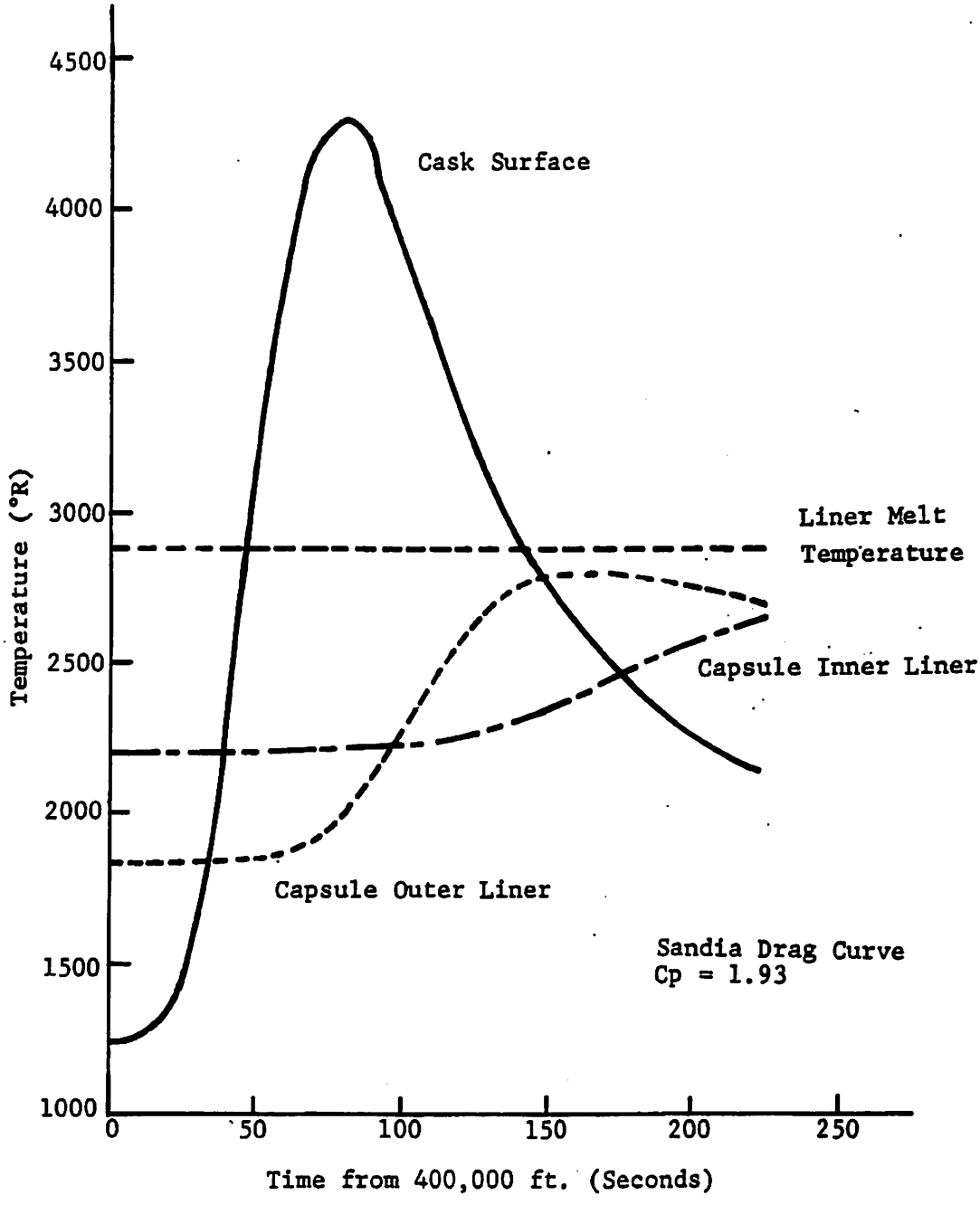

Figure 18. Temperature Response of GLFC and Fuel Capsule from CMA-HERMAN for -6.4° Superorbital Velocity Reentry

results obtained from the HERMAN thermal model alone for the same conditions. A comparison of the two figures indicates that the temperature response obtained in each case is nearly identical. Apparently, this is because for these conditions the heat blockage effect of ablation is directly offset by the increased heating caused by graphite oxidation. Figure 19 shows how the three separate methods of predicting graphite surface temperature compare. The CMA program predicts a peak surface temperature approximately 150°R cooler due to the ablation effects. Figure 20 shows the temperature difference across the graphite heat shield during -6.4° superorbital velocity reentry; it reaches a maximum of 740°F across the 0.35-inch graphite radial thickness.

-38 Degree Supercircular Velocity Reentry

A supercircular velocity reentry at a reentry angle of -38 degrees was analyzed since it represents a maximum probable reentry angle for a mission abort after the LM is inserted into a lunar trajectory.[10] The -38 degree reentries were run for the following cases:

-38° supercircular velocity reentry, LM ascent and descent tanks 100% full.

1. Sandia drag curve, Cp = 1.83
2. Sandia drag curve, Cp = 1.93
3. General Electric drag curve, Cp = 1.93

Some of the input data used for the thermal model for each of the above supercircular velocity reentry cases are shown in Tables XII, XIII and XIV. Included in the tables are time versus altitude, flow regime, convective reference heating, radiative reference heating, heating ratios, and convective cold wall heat input. Figures 21, 22 and 23 show the temperature response of the graphite fuel cask outer surface, fuel capsule inner liner, and fuel capsule outer liner for each of the above cases. As with other trajectories considered, the graphite outer surface peak temperature is lower with the higher pressure coefficient and drag curve. However, the capsule outer liner temperatures are nearly identical throughout each of the -38° reentries, showing practically no dependence upon the changes in the transition drag curve and the pressure coefficient.

The CMA computer code was used to determine the effect of ablation and oxidation for a -38° superorbital velocity reentry trajectory. Figure 24 shows the temperature response of the system obtained from

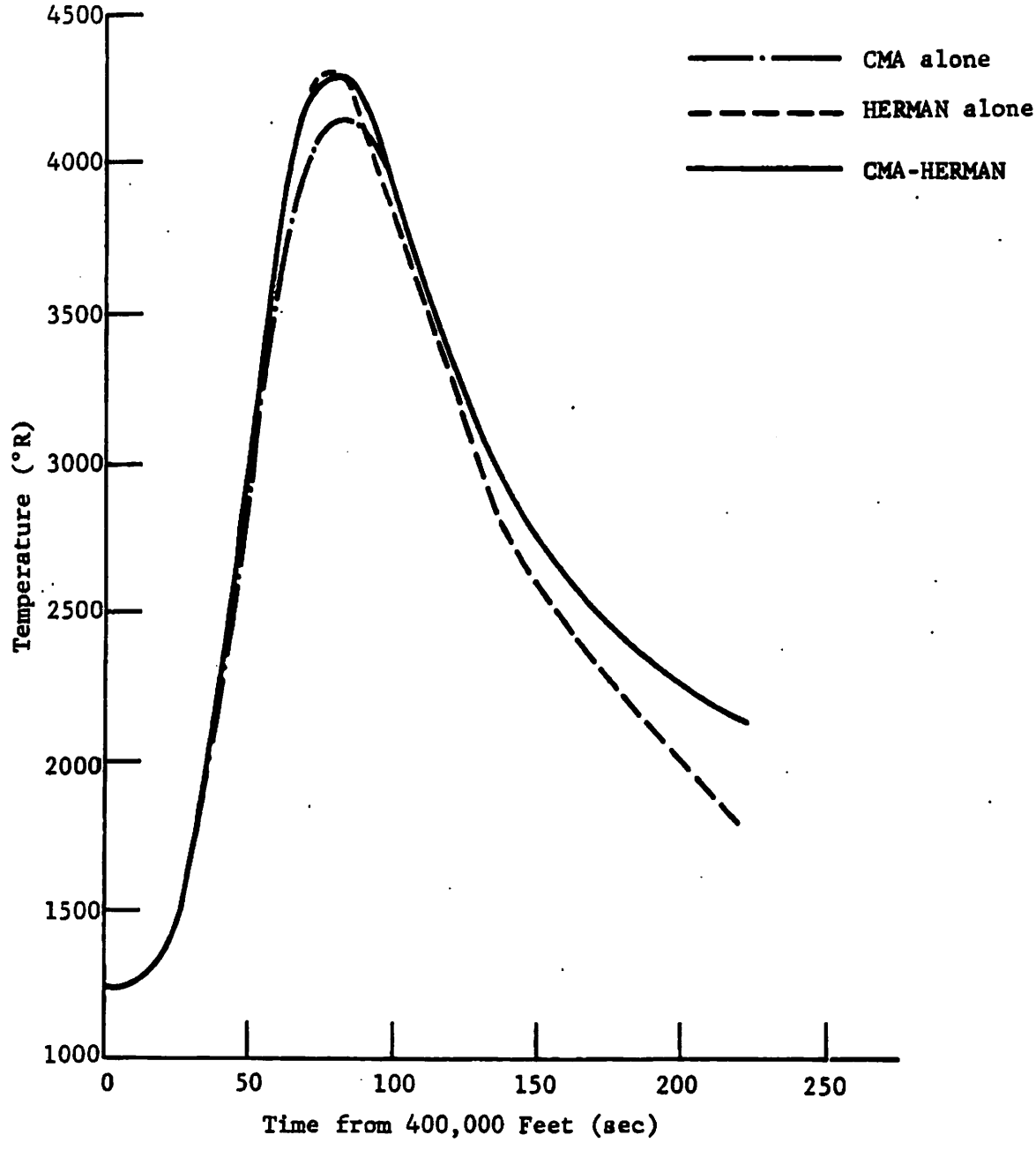

Figure 19. Temperature Response of Cask Surface for -6.4° Superorbital Velocity Reentry

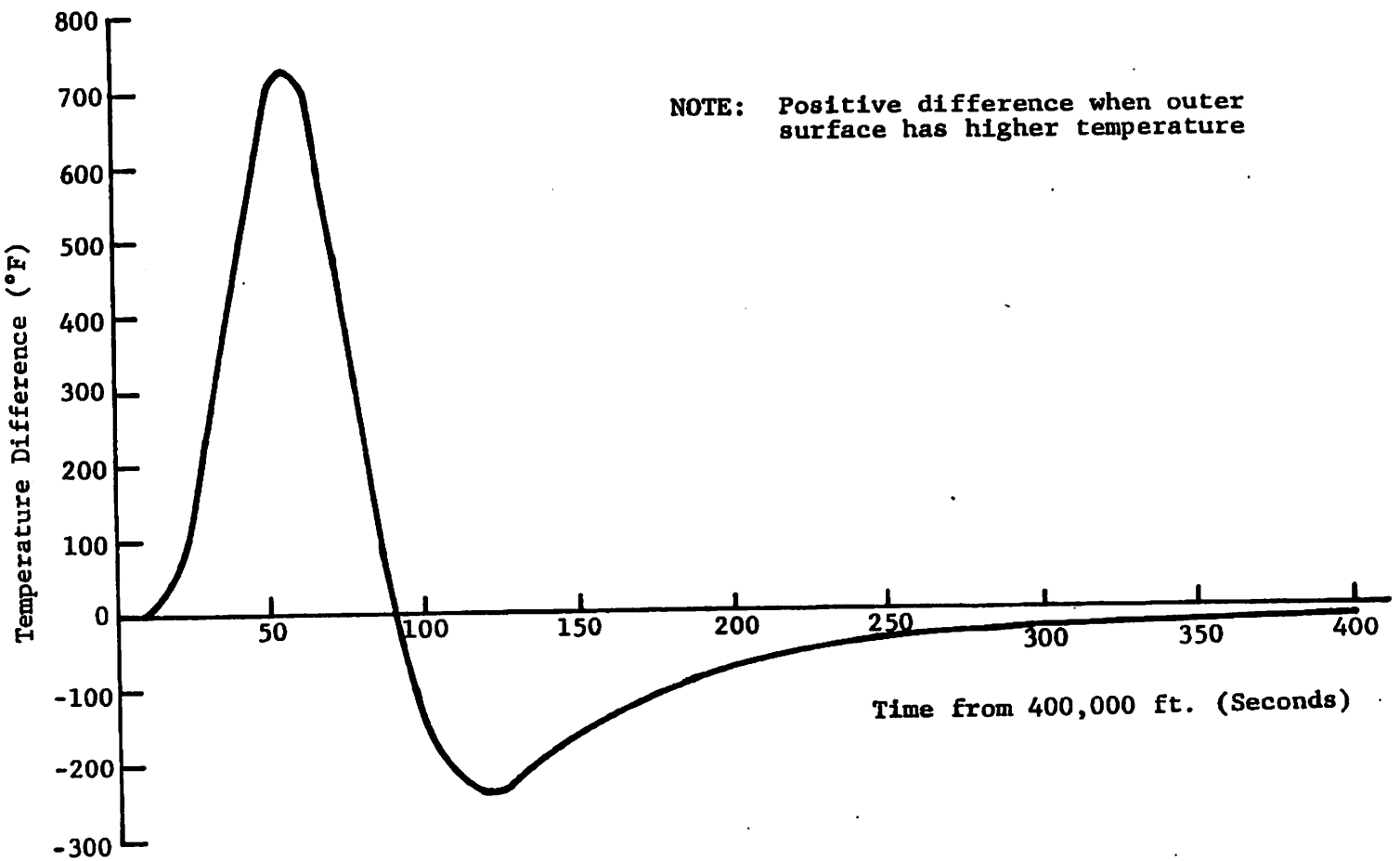

Figure 20. Temperature Difference Across Graphite for -6.4° Superorbital Velocity Reentry

TABLE XII

Heating Rates to GLFC as a Function of Time and Altitude

-38° Superorbital Velocity Reentry
Sandia Drag Curve
Cp = 1.83

Flow Regime	Time (sec)	Altitude (feet)	Convective Reference Heating Rate (BTU/ft^2-sec)	Heating Rate Multiplier (Fq)	Accommodation Coefficient	Cold Wall Heat Input (BTU/ft^2-sec)
Free Molecular	0	400000	1.1	0.3192	0.9	0.316
	1	377610	2.8	0.3192		0.804
	2	355228	7.9	0.3190		2.27
	3	332853	22.5	0.3190		6.46
	4	310481	76.0	0.3190		21.82
Continuum	5	288131	104.4	0.398	Not Applicable	41.55
	6	265788	195.5			77.81
	8	221210	518.3			206.3
	10	177202	1085			431.8
	11	155902	1437			571.9
	12	135747	1712			681.4
	13	117807	1542			613.7
	14	103352	911.4			362.7
	15	92833	379.3			150.9
	16	85546	139.5			55.52
	17	80458	52.9			21.05
	18	76778	22.0			8.76
	20	71820	5.1			2.03
	22	68573	1.7			0.67
	28	62780	0.2			0.08
	50	51526	0.02			0
	270	0	0			0

Radiant Heat Input

Time (sec)	Altitude (feet)	Reference Heating Rate (BTU/ft^2-sec)	Heating Rate Multiplier (Fr)	Radiant Heat Input (BTU/ft^2-sec)
8	221210	15.8	0.125	2.0
9	199071	63.0		7.9
10	177202	216.0		27.0
11	155902	454		56.7
12	135747	442		55.3
13	117807	178		22.3
14	103352	19.4		2.4

TABLE XIII

Heating Rates to GLFC as a Function of Time and Altitude

-38° Superorbital Velocity Reentry
Sandia Drag Curve
Cp = 1.93

Flow Regime	Time (sec)	Altitude (feet)	Convective Reference Heating Rate (BTU/ft^2-sec)	Heating Rate Multiplier (Fq)	Accommodation Coefficient	Cold Wall Heat Input (BTU/ft^2-sec)
Free Molecular	0	400000	1.1	0.3192	0.9	0.32
	1	377610	2.8	0.3192		0.80
	2	355228	7.9	0.3190		2.27
	3	332853	22.5	0.3190		6.46
	4	310487	76.0	0.3190		21.82
Continuum	5	288131	104.4	0.398	Not Applicable	41.55
	6	265789	195.5			77.81
	8	221215	517.9			206.1
	9	199096	762.6			303.5
	10	177240	1079.			429.4
	11	155981	1421.			565.6
	12	135917	1672.			665.5
	13	118134	1475.			587.1
	14	103876	855.5			340.5
	15	93537	352.7			140.4
	16	86374	129.8			51.7
	17	81365	49.5			19.7
	18	77732	20.7			8.24
	20	72824	4.9			1.95
	22	69598	1.6			0.64
	28	63825	0.2			0.08
	50	52579	0.02			0.01
	270	1147	0			0

Radiant Heat Input

Time (sec)	Altitude (feet)	Reference Heating Rate (BTU/ft^2-sec)	Heating Rate Multiplier (F_r)	Radiant Heat Input (BTU/ft^2-sec)
8	221215	15.8	0.125	1.98
9	199096	62.4		7.80
10	177240	211.		26.38
11	155981	425.		53.12
12	135917	385.		48.13
13	118134	150.		18.75
14	103876	15.1		1.89
15	93537	0		0

TABLE XIV

Heating Rates to GLFC as a Function of Time and Altitude

-38° Superorbital Velocity Reentry
General Electric Drag Curve
Cp = 1.93

Flow Regime	Time (sec)	Altitude (feet)	Convective Reference Heating Rate (BTU/ft^2-sec)	Heating Rate Multiplier (Fq)	Accommodation Coefficient	Cold Wall Heat Input (BTU/ft^2-sec)
Free Molecular	0	400000	1.1	0.3192	0.9	0.32
	1	377610	2.8	0.3192		0.80
	2	355288	7.9	0.3190		2.27
	3	332853	22.5	0.3190		6.46
	4	310487	76.0	0.3190		21.82
Continuum	5	288131	104.4	0.398	Not	41.55
	6	265788	195.5		Applicable	77.81
	8	221225	516.9			205.7
	9	199113	759.7			302.4
	10	177294	1072.			426.6
	11	156083	1406.			559.6
	12	136093	1643.			773.3
	13	118407	1436.			571.5
	14	104252	826.7			329.0
	15	93996	340.1			135.4
	16	86887	125.4			49.91
	17	81909	47.96			19.09
	18	78294	20.13			8.01
	20	73402	4.77			1.90
	22	70183	1.56			0.62
	28	64413	0.17			0.07
	50	53167	0.02			0
	280	327	0			0

Radiant Heat Input

Time (sec)	Altitude (feet)	Reference Heating Rate (BTU/ft^2-sec)	Heating Rate Multiplier (Fr)	Radiant Heat Input (BTU/ft^2-sec)
7	243475	3.21	0.125	0.40
8	221225	15.7		1.96
9	199113	61.5		7.69
10	177294	206.		25.75
11	156083	399.		49.88
12	136093	348.		43.50
13	118407	135.		16.87
14	104252	13.3		1.66
15	93996	0.4		0.05

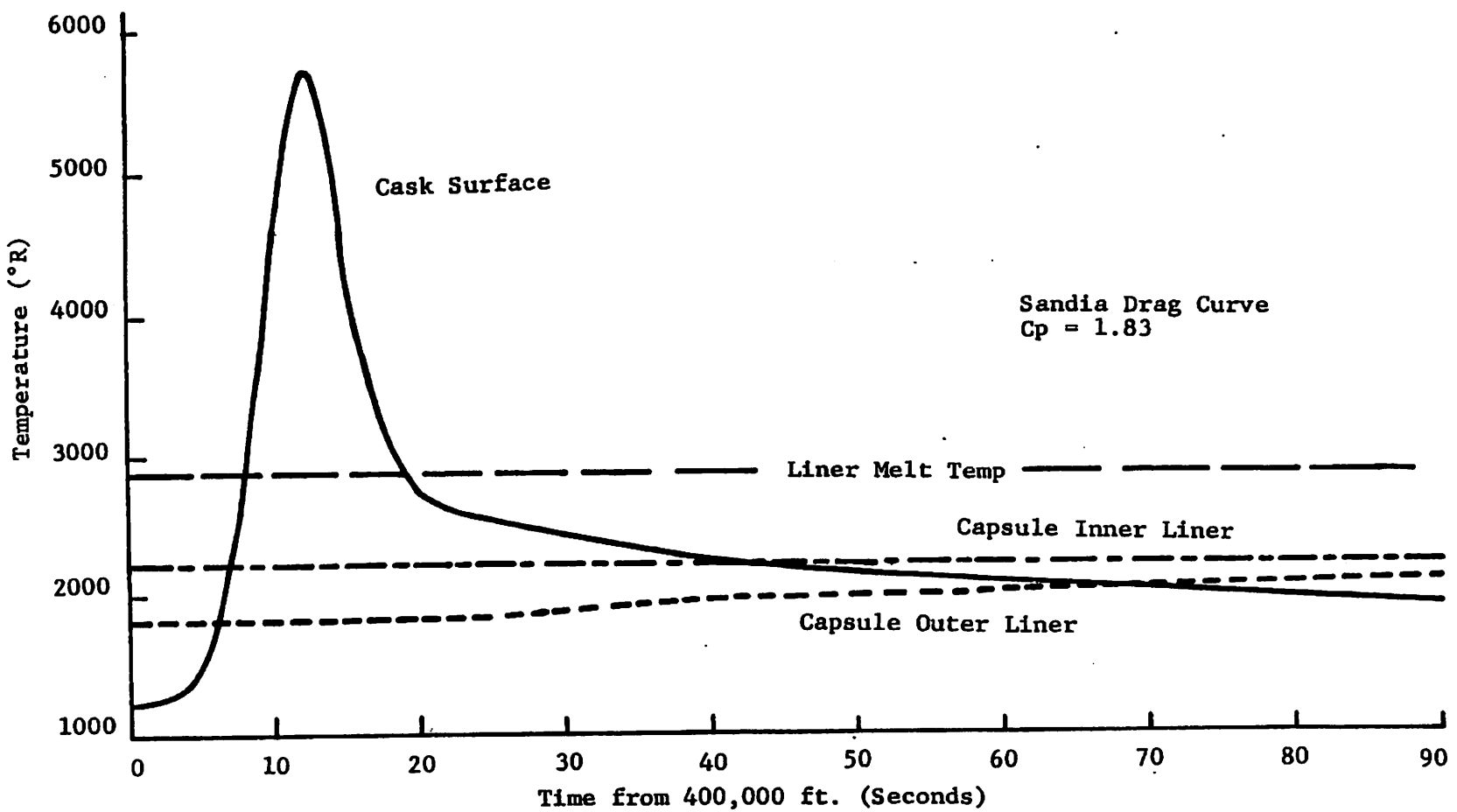

Figure 21. Temperature Response of GLFC and Fuel Capsule for -38° Superorbital Velocity Reentry

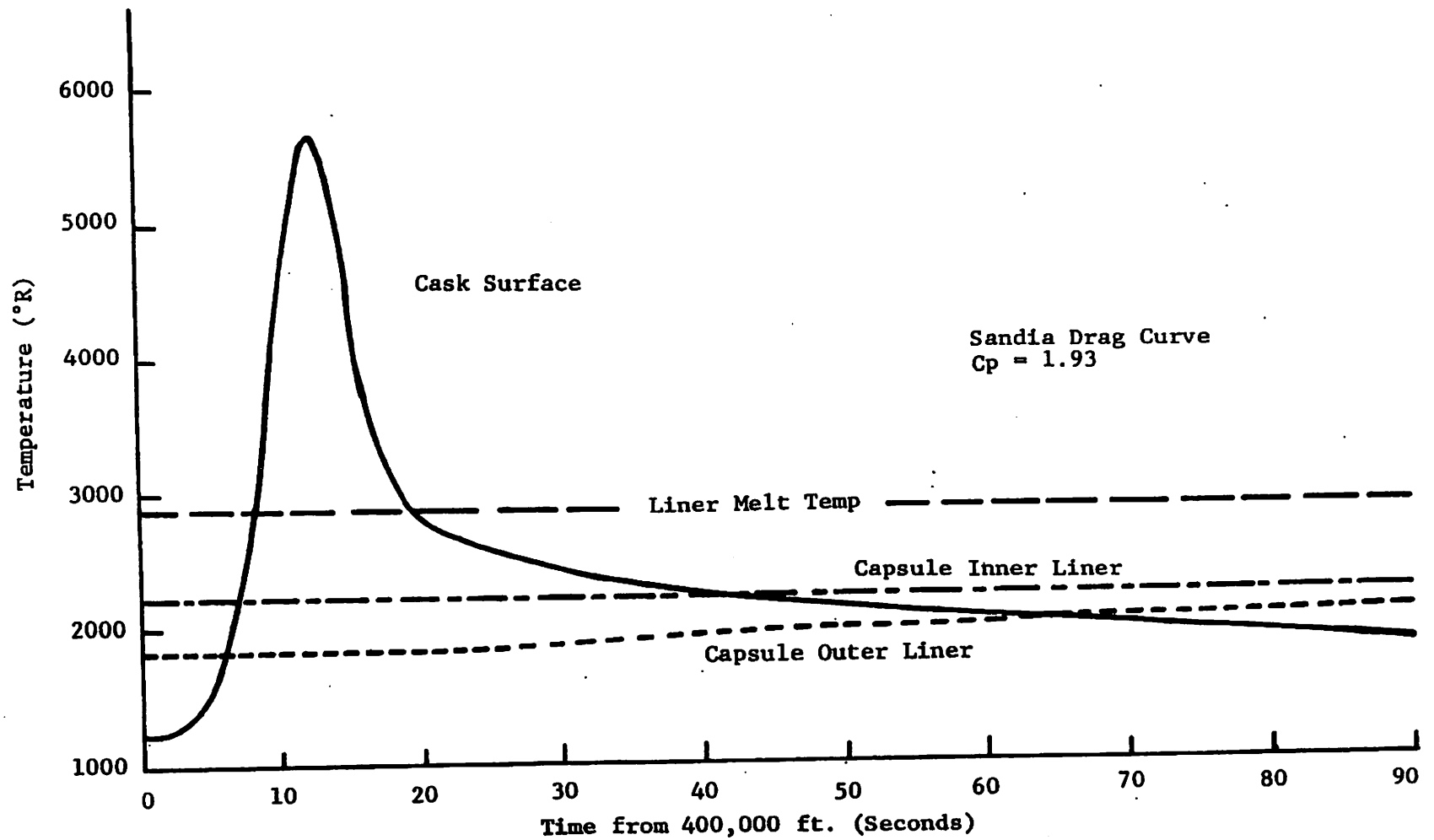

Figure 22. Temperature Response of GLFC and Fuel Capsule for -38° Superorbital Velocity Reentry

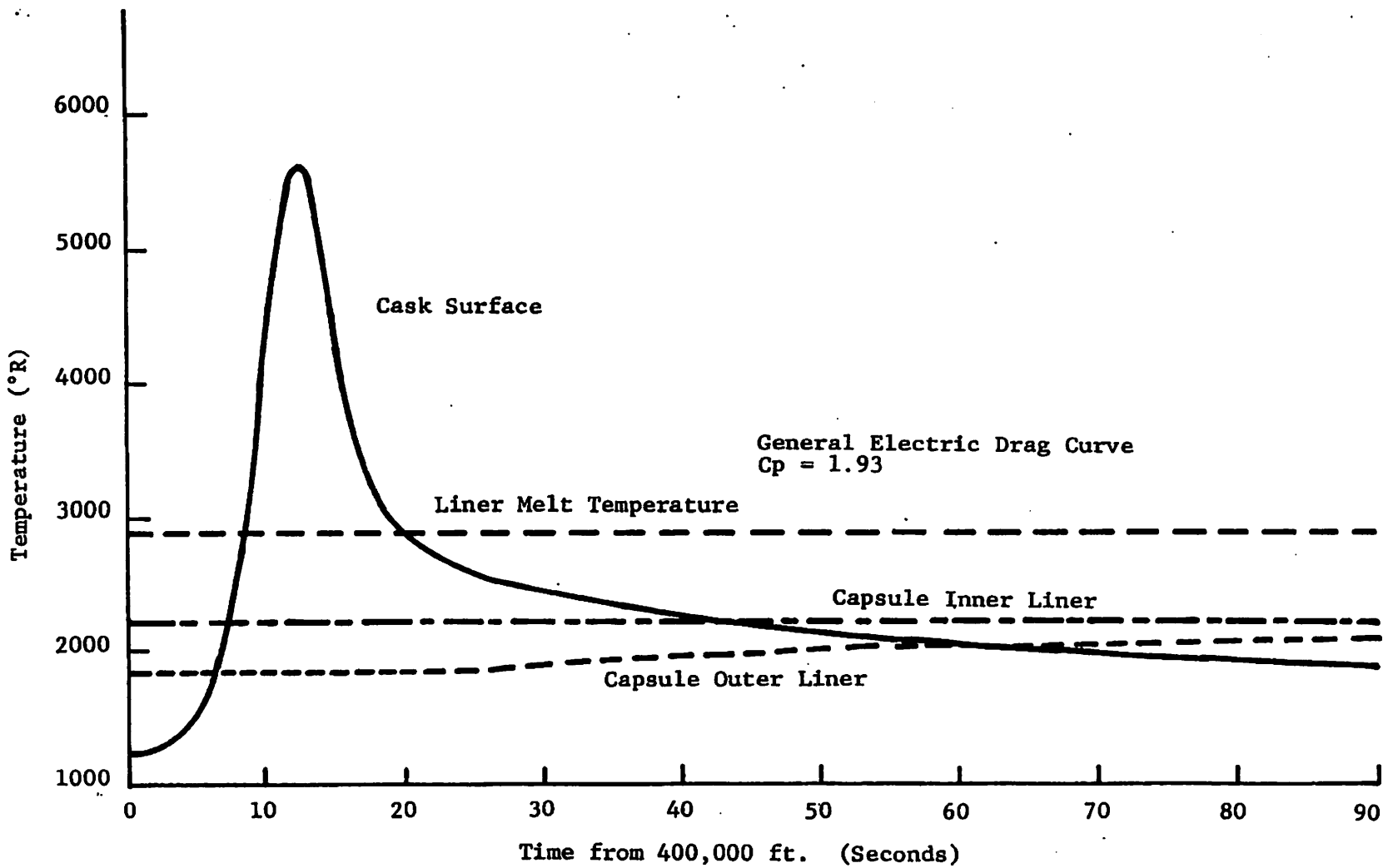

Figure 23. Temperature Response of GLFC and Fuel Capsule for -38° Superorbital Velocity Reentry

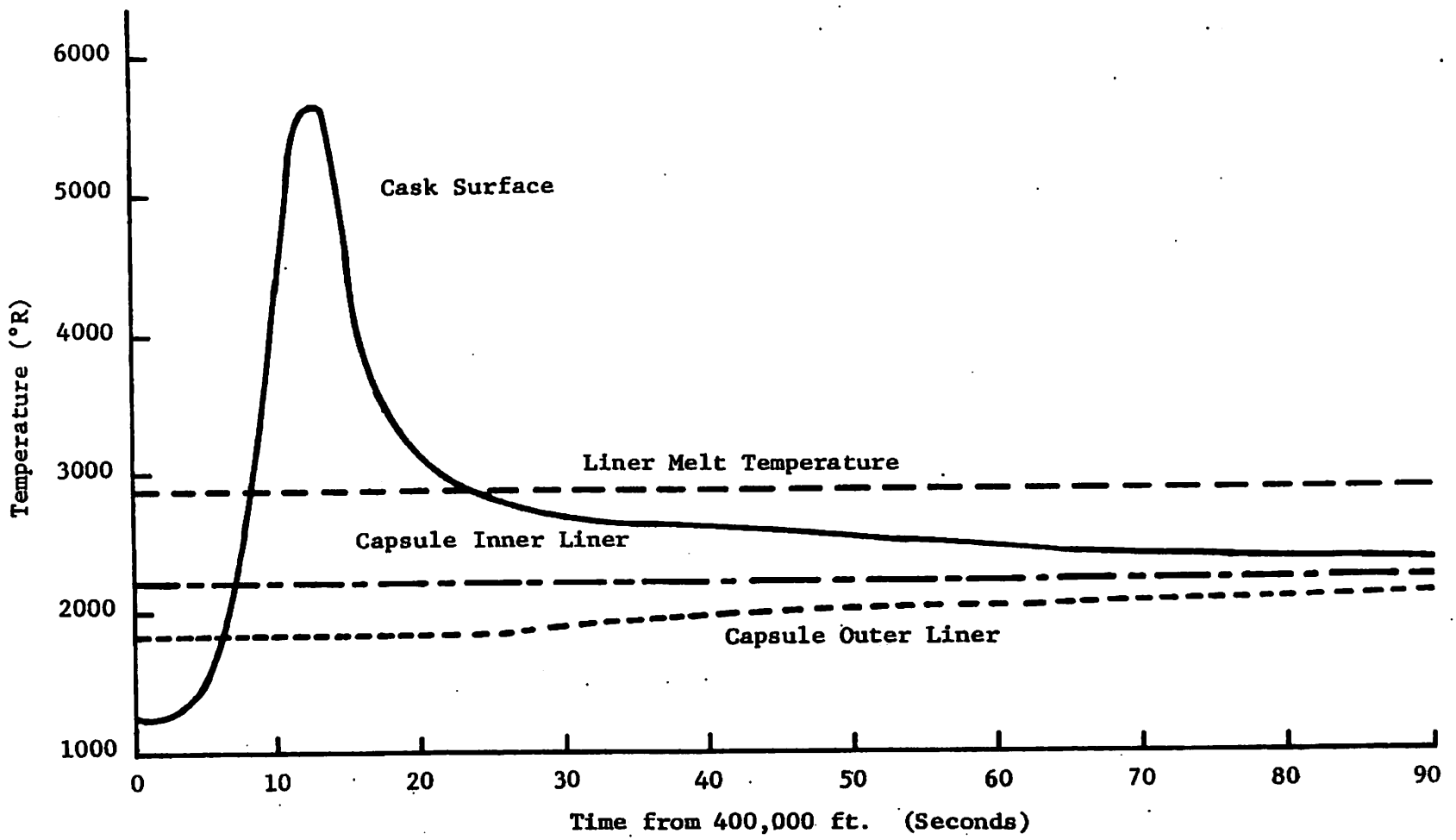

Figure 24. Temperature Response of GLFC and Fuel Capsule from CMA-HERMAN for -38° Superorbital Reentry

using the corrected heat flux from CMA as input to the HERMAN thermal model. A comparison with Figure 22, which shows the results obtained for the same case using the HERMAN thermal model alone, indicates that the temperature response of the fuel capsule is the same in each case. This is caused primarily by the short reentry time. The heat pulse is so short that the fuel capsule feels no effect from it, regardless of whether or not the ablation effects are taken into account.

Figure 25 compares the three methods of predicting the graphite outer surface temperature for this steep reentry condition. Ablation and oxidation effects are quite pronounced for this reentry trajectory. The CMA program predicts peak graphite wall temperatures approximately 800°R lower than the HERMAN thermal model. This large temperature difference is caused primarily by the ablation heat blockage effect. At high temperatures, the CMA program uses a slightly higher graphite emissivity than does the HERMAN thermal model and this contributes also to the temperature difference. The CMA program predicts graphite surface temperatures approximately 700°R higher after the heat pulse when temperatures level off. This is caused by the additional heat input to the CMA model caused by graphite oxidation.

The -38° superorbital velocity reentry creates a high heat pulse of short duration. This heat pulse causes a large temperature difference across the 0.35-inch graphite wall (Figure 26) and reaches a maximum of 2970°R.

Conclusions

The results indicate that for all three classes of reentry trajectories considered (orbital decay, -6.4° superorbital velocity reentry, and -38° superorbital velocity reentry) the different transition drag curves and pressure coefficients used in the trajectories had very little effect upon the temperature response of the system. The reaction kinetics of the graphite during reentry had almost no effect during orbital decay reentry and only a small effect during the -6.4° superorbital velocity reentry. During the -38° superorbital velocity reentry, the graphite reaction kinetics had a large effect upon the temperature response of the graphite surface; however, this short time trajectory did not allow these effects to propagate inward and thus the interior temperature response was unaffected.

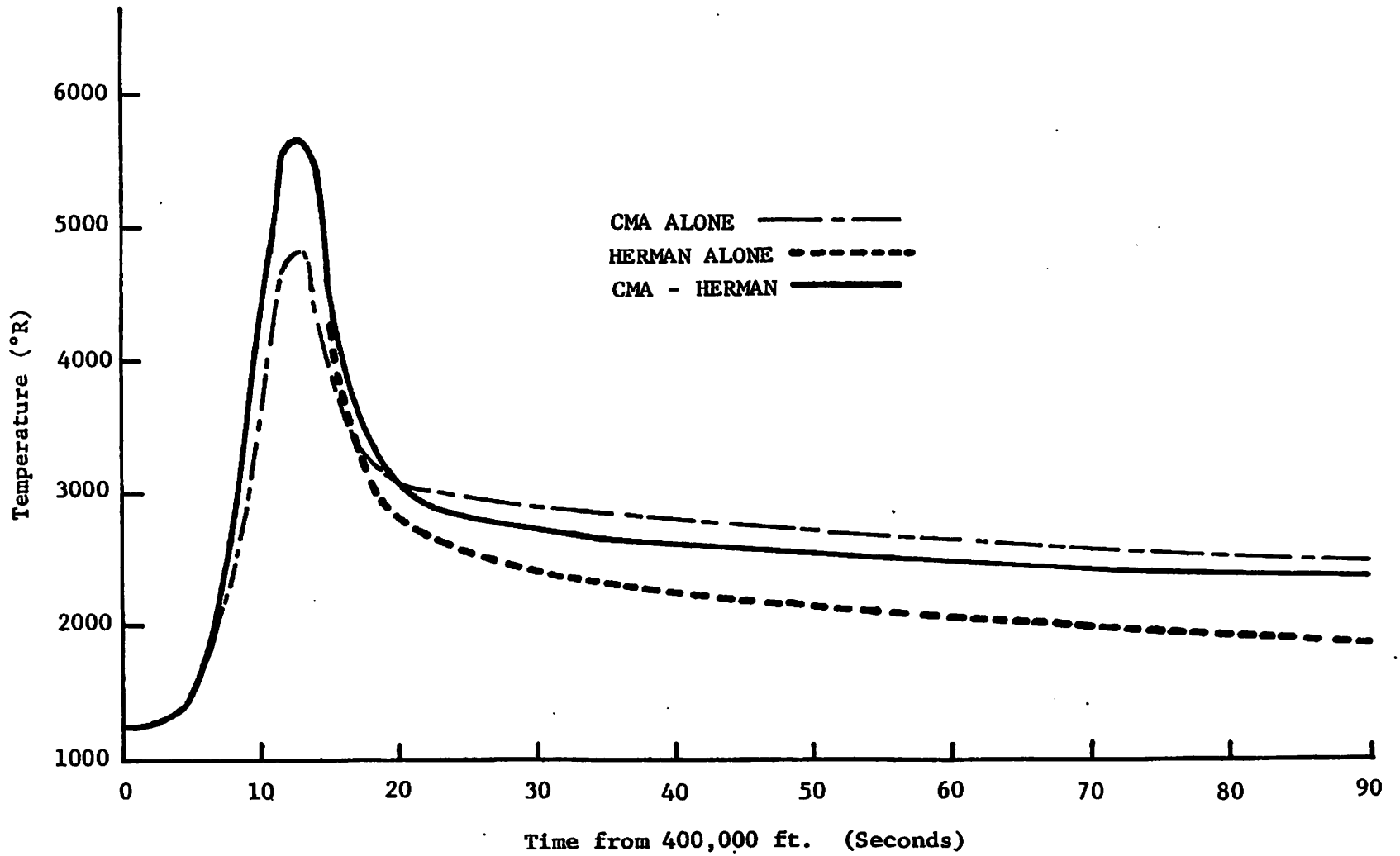

Figure 25. Temperature Response of Cask Surface for -38° Superorbital Reentry

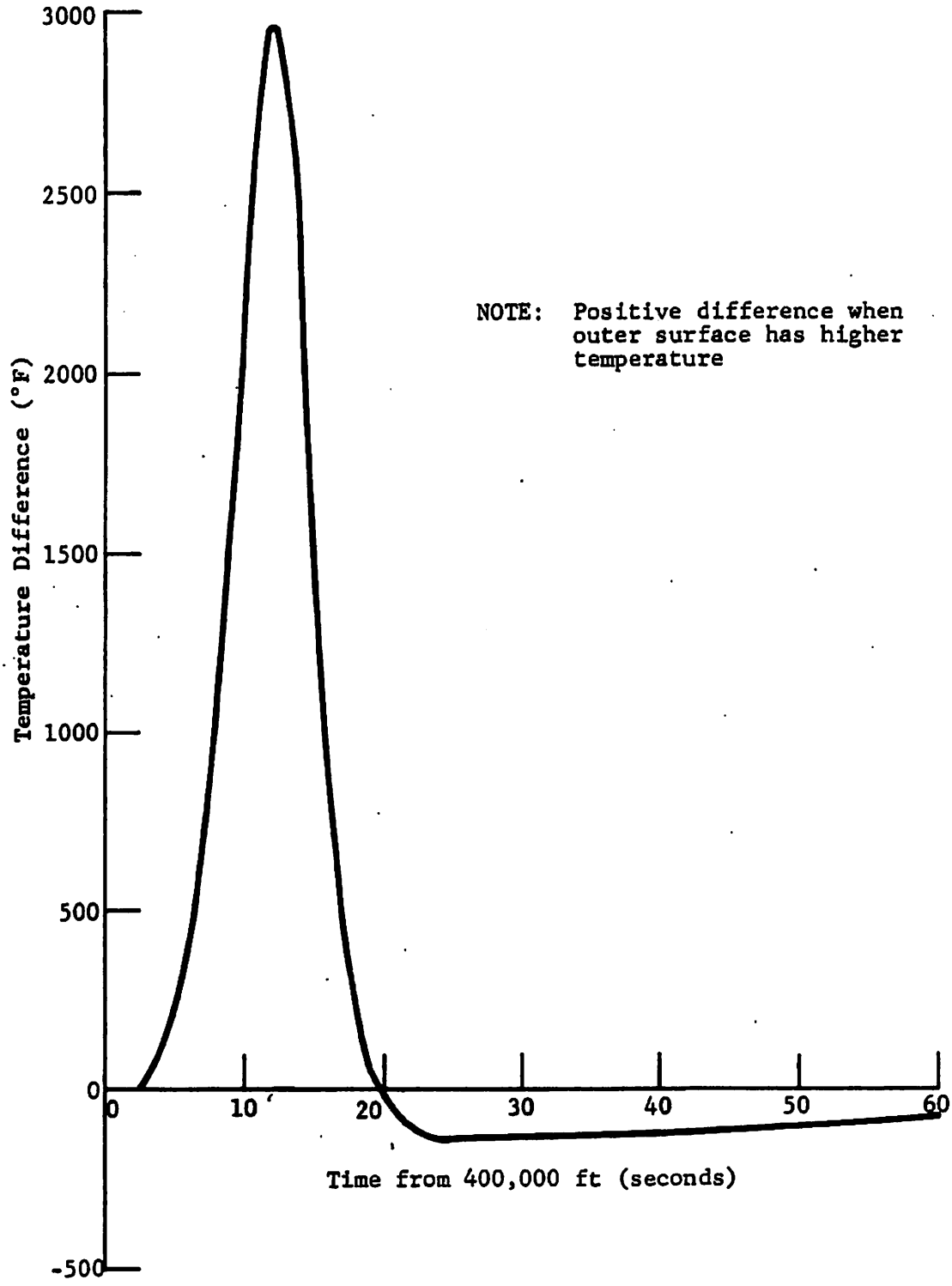

Figure 26. Temperature Difference Across Graphite for -38° Superorbital Reentry

The fuel capsule inner and outer liner reached their maximum temperatures during orbital decay reentry. The outer liner maximum temperature was approximately 100-150°R below the melt condition, and the inner liner just reached melt temperature. For both superorbital reentries, the fuel capsule liners remained well below the melt temperature.

The temperature difference across the graphite heat shield was small for orbital decay, but reached 740°F for -6.4° superorbital reentry and 2970°F for -38° superorbital reentry. This 2970°F temperature difference is very large for the 0.35-inch graphite thickness, and the thermal stresses will be significant. A complete thermal stress analysis should be performed to determine if the graphite can withstand such a temperature difference.

REFERENCES

1. SC-RR-66-611, Aerothermodynamic Analysis of the SNAP-27 Fuel Cask, S. McAlees, Jr., R. D. Klett, B. E. Pierce, D. W. Larson, J. T. Stephens, and H. R. Spahr, Sandia Laboratory, Albuquerque, New Mexico, September 1966.

2. SC-RR-66-2651, Aerothermodynamic and Structural Analysis of the SNAP-27 Fuel Cask, R. E. Berry, R. D. Klett, D. W. Larson, and H. R. Spahr, Sandia Laboratory, Albuquerque, New Mexico, January 1967.

3. SC-RR-67-150, Aerodynamic and Trajectory Analyses of a SNAP-27 Graphite Fuel Cask, H. R. Spahr, Sandia Laboratory, Albuquerque, New Mexico, May 1967.

4. General Electric Company, Missile and Space Division, Drawing 15227-47E301134, Sheet 1.

5. Instructions for Using the Sandia Heat Transfer Program, HERMAN, F. O. Lane, Sandia Laboratory, Albuquerque, New Mexico, January 27, 1965.

6. SC-RR-64-2141, Drag Coefficients and Heating Ratios for Right Circular Cylinders in Free-Molecular and Continuum Flow From Mach 10 to 30, R. D. Klett, Sandia Laboratory, Albuquerque, New Mexico, December, 1964.

7. SC-DR-65-511, The TTA Generalized Rigid Body Trajectory Program for Digital Computer, J. A. F. Allensworth, Sandia Laboratory, Albuquerque, New Mexico, August 1966.

8. Radiative Heating of Vehicles Entering the Earth's Atmosphere, Bradford H. Wick, NASA Ames Research Center, Moffet Field, California, April 3, 1962.

9. Minutes of Meeting on Aerothermodynamic Analysis of SNAP-27 GLFC, Sandia Laboratory, Albuquerque, New Mexico, September 13, 1967.

10. Minutes of the SNAP-27 Reentry Analysis Meeting held at the Manned Spacecraft Center, July 27, 1966. Enclosure 7

11. SC-M-66-377, Operation Instructions for Charring Material Ablation Code, F. W. Bolek and D. S. McVey, Sandia Laboratory, Albuquerque, New Mexico, August 1966.

12. NASA TN D-968, Charts Depicting Kinematic and Heating Parameters for a Ballistic Reentry at Speeds of 26,000 to 45,000 Feet Per Second, U. M. Lovelace, Langley Research Center, October, 1961.

APPENDIX A

APPENDIX A

Material Properties Used in the Thermal Model

Graphite*

Density = 88 lb/ft^3

Emissivity = 0.8 (at all temperatures)**

Specific Heat, Cp

Temperature (°F)	Cp (BTU/lb-°F)
70	0.22
1000	0.39
4000	0.53
7540	0.53

Thermal Conductivity, K

Temperature (°F)	K (BTU/HR-Ft-°F)
165	4.85
565	5.22
965	5.50
1365	5.76
1965	6.04
2365	6.15
2965	6.30
4165	6.66
5665	6.92
7540	7.50

*Pyrocarb 406

**The CMA runs allowed emissivity to vary with temperature.

Silver

Density = 657 lb/ft^3

Emissivity (High emissivity coating) = 0.8

Specific Heat = 0.056 BTU/lb-°F

Thermal Conductivity, K

Temperature (°F)	K (BTU/HR-Ft-°F)
740	208
1761	208

Melt Temperature = 1761.4 °F

Heat of Fusion = 43.9 BTU/lb

Columbium

Density = 541 lb/ft^3

Emissivity (coated) = 0.8

Specific Heat = 0.074 BTU/lb-°F

Thermal Conductivity, K

Temperature (°F)	K (BTU/HR-Ft-°F)
0	32
1200	38
4000	32

Silicon Dioxide

Density = 114 lb/ft^3

Emissivity (coated) = 0.8

Specific Heat, Cp

Temperature (°F)	Cp (BTU/lb-°F)
0	0.18
500	0.24
1500	0.288
2000	0.30
5000	0.30

Thermal Conductivity, K

Temperature (°F)	K (BTU/HR-Ft-°F)
0	0.08
500	0.25
800	0.32
1300	0.36
1500	0.41
1600	0.45
1800	0.57
2000	0.65
5000	0.90

Haynes 25

Density = 570 lb/ft^3

Emissivity (iron titanate coating) = 0.85

Specific Heat, Cp

Temperature (°F)	Cp (BTU/lb-°F)
60	0.092
2425	0.19

Thermal Conductivity, K

Temperature (°F)	K (BTU/HR-Ft-°F)
100	5.59
500	8.10
900	10.61
1300	13.10
1700	15.90
2100	19.50
2425	23.00

Melting Range = 2425 - 2570 °F

Heat of Fusion = 115 BTU/lb

Plutonium Dioxide ($Pu^{238}O_2$) Microspheres

Density = 662 lb/ft^3

Specific Heat, Cp

Temperature (°F)	Cp (BTU/lb-°F)
240	0.0662
840	0.0734
3000	0.0835
4000	0.0835

Thermal Conductivity, K

Temperature (°F)	K (BTU/HR-Ft-°F)
1000	0.46
1500	0.62
1700	0.68
4000	0.75

DISTRIBUTION:
U. S. Atomic Energy Commission
Division of Space Nuclear Systems
Space Electric Power Office
Washington, D. C. 20545
Attn: G. A. Newby (1)
Assistant Director
G. P. Dix, Chief (1)
Safety Branch
R. S. Decker, Jr., Chief (1)
Safety Branch
R. T. Carpenter, Chief (1)
Isotope Power Sys. Branch
J. A. Powers, Chief (1)
Isotopes and Matls. Branch
C. Johnson, Chief (1)
Reactor Power Sys. Branch

U. S. Atomic Energy Commission
Division of Isotope Development
Washington, D. C. 20545

U. S. Amotic Energy Commission
Director of Regulation
Washington, D. C. 20545
Attn: C. K. Beck (1)
Deputy Director
F. D. Anderson (1)
Regulation

U. S. Atomic Energy Commission
Division of Biology and Medicine
Washington, D. C. 20545
Attn: J. Z. Holland, Chief (1)
Fallout Studies Branch
H. D. Bruner, Asst. Dir. (1)
Med. and Health Research

U. S. Atomic Energy Commission
Space Nuclear Propulsion Office
Albuquerque Extension
Albuquerque Operations Office
P. O. Box 5400
Albuquerque, New Mexico 87115
Attn: H. P. Smith

U. S. Atomic Energy Commission
Albuquerque Operations Office
P. O. Box 5400
Albuquerque, New Mexico 87115
Attn: S. A. Upson, Director (1)
Non-Nuclear Activities Div.
J. F. Burke, Director (1)
Operational Safety Division

AEC Site Representative
National Aeronautics and Space Adm.
Manned Spacecraft Center
Houston, Texas 77058
Attn: W. C. Remini
Bldg. 16, Code ZS-5

DISTRIBUTION: (cont)

General Electric Company
Valley Forge Space Technology Ctr.
P. O. Box 8555
Philadelphia, Pennsylvania 19101
Attn: S. M. Scala, Room M9539 (1)
Space Sciences Lab
T. F. Widmer (1)
Advanced Nuclear Sys. Opr.

Deputy I. G. for Insp. and Safety
USAF
Kirtland Air Force Base
New Mexico 87117
Attn: Col. D. C. Jameson (AFINSR)

Los Alamos Scientific Laboratory
P. O. Box 1663
Los Alamos, New Mexico 87544
Attn: Dr. L. D. P. King (1)
Dr. Wright Langham (1)
C. F. Metz, CMB-1 (1)
F. W. Schonfeld, CMF-5 (1)

Thomas B. Kerr
Code RNS
National Aeronautics and Space Adm.
Washington, D. C. 20545

National Aeronautics and Space Adm.
Ames Research Center
Moffet Field, California
Attn: Glenn Goodwin

U. S. Naval Radiological Defense Lab.
San Francisco, California 94135
Attn: S. Z. Mikhail
Nuclear Systems Group

National Aeronautics and Space Adm.
Goddard Space Flight Center
Glenn Dale Road
Greenbelt, Maryland 20771
Attn: A. W. Fihelly
Nimbus Project

Naval Facilities Engineering Command
Department of the Navy, Code 042
Washington, D. C. 20390
Attn: Graham Hagey

Space Nuclear Propulsion Office
Lewis Research Center
21000 Brookpark Road
Cleveland, Ohio 44135
Attn: L. Nichols

U. S. Public Health Service
Nat. Ctr. for Radiological Health
1901 Chapman Avenue
Rockville, Maryland 20852
Attn: Nuclear Facilities Section

DISTRIBUTION (cont):

Dr. D. W. Sherwood
National Aeronautics and Space Adm.
Manned Spacecraft Center (MSC-TD)
Houston, Texas 77058

D. B. Shuster, 1200
J. R. Banister, 5270
J. D. Shreve, 5271
L. E. Lamkin, 7300
G. A. Fowler, 9000
H. E. Viney, 9130
R. C. Maydew, 9320
L. A. Hopkins, Jr., 9500
V. E. Blake, 9510
H. E. Hansen, 9511
S. L. Jeffers, 9512
S. McAlees, Jr., 9513
D. W. Larson, 9513 (2)
J. D. Appel, 9514
J. D. Appel, 9514 (ARPIC) (2)
R. J. Everett, 9515
A. J. Clark, 9520
J. W. McKiernan, 9521
J. Jacobs, 9522
B. F. Hefley, 8232 (5)
B. R. Allen, 3421
C. H. Sproul, 3428-2 (10)
L. C. Baldwin, 3412
L. L. Alpaugh, 3412